



OPEN ACCESS

EDITED BY

Joachim H. R. Lübke,
Helmholtz Association of German Research
Centres (HZ), Germany

REVIEWED BY

Alev Erisir,
University of Virginia, United States
Wen-Jun Gao,
Drexel University, United States
Mira Jakovcevski,
Max Planck Institute of Psychiatry (MPI),
Germany

*CORRESPONDENCE

Amy F. T. Arnsten
✉ amy.arnsten@yale.edu

RECEIVED 30 December 2024

ACCEPTED 19 March 2025

PUBLISHED 04 April 2025

CITATION

Joyce MKP, Datta D, Arellano JI, Duque A,
Morozov YM, Morrison JH and
Arnsten AFT (2025) Contrasting patterns of
extrasynaptic NMDAR-GluN2B expression in
macaque subgenual cingulate and
dorsolateral prefrontal cortices.
Front. Neuroanat. 19:1553056.
doi: 10.3389/fnana.2025.1553056

COPYRIGHT

© 2025 Joyce, Datta, Arellano, Duque,
Morozov, Morrison and Arnsten. This is an
open-access article distributed under the
terms of the [Creative Commons Attribution
License \(CC BY\)](#). The use, distribution or
reproduction in other forums is permitted,
provided the original author(s) and the
copyright owner(s) are credited and that the
original publication in this journal is cited, in
accordance with accepted academic
practice. No use, distribution or reproduction
is permitted which does not comply with
these terms.

Contrasting patterns of extrasynaptic NMDAR-GluN2B expression in macaque subgenual cingulate and dorsolateral prefrontal cortices

Mary Kate P. Joyce¹, Dibyadeep Datta², Jon I. Arellano¹,
Alvaro Duque¹, Yury M. Morozov¹, John H. Morrison^{3,4} and
Amy F. T. Arnsten^{1*}

¹Department of Neuroscience, Yale Medical School, New Haven, CT, United States, ²Department of
Psychiatry, Yale Medical School, New Haven, CT, United States, ³Department of Neurology, University
of California, Davis, Davis, CA, United States, ⁴California National Primate Research Center, University
of California, Davis, Davis, CA, United States

Expression of the N-methyl-D-aspartate receptor, particularly when containing the GluN2B subunit (NMDAR-GluN2B), varies across the prefrontal cortex (PFC). In humans, the subgenual cingulate cortex (SGC) contains among the highest levels of NMDAR-GluN2B expression, while the dorsolateral prefrontal cortex (dlPFC) exhibits a more moderate level of NMDAR-GluN2B expression. NMDAR-GluN2B are commonly associated with ionotropic synaptic function and plasticity and are essential to the neurotransmission underlying working memory in the macaque dlPFC in the layer III circuits, which in humans are afflicted in schizophrenia. However, NMDAR-GluN2B can also be found at extrasynaptic sites, where they may trigger distinct events, including some linked to neurodegenerative processes. The SGC is an early site of tau pathology in sporadic Alzheimer's disease (sAD), which mirrors its high NMDAR-GluN2B expression. Additionally, the SGC is hyperactive in depression, which can be treated with NMDAR antagonists. Given the clinical relevance of NMDAR in the SGC and dlPFC, the current study used immunoelectron microscopy (immunoEM) to quantitatively compare the synaptic and extrasynaptic expression patterns of NMDAR-GluN2B across excitatory and inhibitory neuron dendrites in rhesus macaque layer III SGC and dlPFC. We found a larger population of extrasynaptic NMDAR-GluN2B in dendrites of putative pyramidal neurons in SGC as compared to the dlPFC, while the dlPFC had a higher proportion of synaptic NMDAR-GluN2B. In contrast, in putative inhibitory dendrites from both areas, extrasynaptic expression of NMDAR-GluN2B was far more frequently observed over synaptic expression. These findings may provide insight into varying cortical vulnerability to alterations in excitability and neurodegenerative forces.

KEYWORDS

extrasynaptic NMDA receptor, GluN2B (NMDA receptor subunit NR2B), subgenual anterior cingulate cortex, dorsolateral prefrontal cortex, area 25, area 46, neurodegeneration, major depression (MDD)

Introduction

The NMDAR is a di- or tri-heteromeric complex that typically contains two GluN1 subunits and a combination of GluN2B or GluN3 subunits, which define the biophysical properties of the receptor (Paoletti et al., 2013; Wyllie et al., 2013). The GluN2B subunit (encoded by the gene *GRIN2B*) confers slow closing kinetics and high calcium permeability, thus allowing significant calcium entry into the neuron (Erreger et al., 2005; Glasgow et al., 2015). In humans, *GRIN2B* expression increases along a sensory-association cortical gradient, which is correlated with cortical hierarchy (Burt et al., 2018), and similar to a cortical gradient of increasing intrinsic timescales for local processing (Murray et al., 2014). *GRIN2B* expression is thus lowest in sensory areas such as primary visual and somatosensory cortex, intermediate levels in association cortices such as the dorsolateral prefrontal cortex (dlPFC), and highest in limbic areas such as the subgenual cingulate cortex (SGC) (Burt et al., 2018; Yang et al., 2018), an area associated with mood, visceromotor function, and hyperactivity in depression (Mayberg et al., 2005; Alexander et al., 2019a). *GRIN2B* expression also increases within the frontal pole across primate phylogeny, suggesting a prominent role in higher cognition (Muntané et al., 2015). Studies in macaque dlPFC suggest that the long calcium influx conferred by the NMDAR-GluN2B subunit in layer III dlPFC pyramidal cell recurrent circuits is critical to maintaining persistent firing in the absence of external sensory stimulation during the delay epoch of a spatial working memory task (Lisman et al., 1998; Wang M. et al., 2013; Yang et al., 2018; Yang et al., 2021). Consistent with the critical role of NMDAR-GluN2B in delay-related firing in dlPFC, post-embedding immunoEM has detected prominent NMDAR-GluN2B expression within the post-synaptic density (PSD) in spines of layer III (Wang M. et al., 2013). Higher expression of NMDAR-GluN2B in limbic association areas may support neural constructs that require longer continuity than working memory, such as mood and emotion (Yang et al., 2021).

NMDAR can also be extrasynaptic, where they may serve distinct functions (Petralia, 2012; Groc and Choquet, 2020; Petit-Pedrol and Groc, 2021). The presence of the GluN2B subunit has been prominently associated with extrasynaptic expression (Tovar and Westbrook, 1999; Papouin et al., 2012), although other evidence suggests that extrasynaptic subunit specificity is not quite so clear cut (Thomas et al., 2006; Harris and Pettit, 2007; Kortus et al., 2023), and that expression patterns could be area-specific or species-specific (e.g., Harris and Pettit, 2007; Petralia et al., 2010; Wang M. et al., 2013). Extrasynaptic NMDAR has been associated with events distinct from synaptic NMDAR (reviewed in Hardingham and Bading, 2010; Gladding and Raymond, 2011; Parsons and Raymond, 2014) and in particular with a host of very detrimental events in states of acute injury, cellular distress, and neurodegeneration (e.g., Hardingham et al., 2002; Zong et al., 2022).

Memantine, a low-affinity, non-competitive antagonist and open channel blocker of the NMDAR, is an FDA-approved drug with modest efficacy in treating moderate-to-severe sAD (Kim et al., 2024) and is hypothesized to target extrasynaptic NMDAR (Xia et al., 2010). Furthermore, other non-specific NMDA antagonists, such as ketamine, and GluN2B-specific antagonists may target extrasynaptic populations of NMDAR to exert rapid-acting antidepressant effects (Miller et al., 2014; Miller et al., 2016; Brown and Gould, 2024; Krystal et al., 2024), although ketamine can also mimic schizophrenia by impairing dlPFC cognitive function (Beck et al., 2020). Given the

significance of NMDAR-GluN2B to dlPFC and SGC function, as well as its relevance in psychiatric disorders (Yang et al., 2021), it is critical to understand the distribution of NMDAR-GluN2B across synaptic and extrasynaptic membrane domains of diverse cell types in these circuits. Variability in NMDAR membrane expression across the PFC landscape may produce mixed effects during the systemic administration of pharmacological NMDAR agents.

Very few studies have examined NMDAR-GluN2B in primate PFC. As mentioned above, post-embedding immunoEM demonstrated NMDAR-GluN2B within glutamate-like synapses on spines in layer III dlPFC (Wang M. et al., 2013). Post-embedding immunoEM is ideal for identifying synaptic proteins because it provides superior access to the PSD (Petralia and Wang, 2021). For example, Wang M. et al. (2013) showed prominent NMDAR-GluN2B labeling within the PSD. However, the post-embedding process can degrade extra-synaptic membranes, and thus the selective labeling of the PSD in Wang M. et al. (2013) may be an accurate reflection of GluN2B selective localization or may be impacted by inherent constraints of the technique. Pre-embedding immunoEM, on the other hand, often provides superior preservation of ultrastructure, in particular extrasynaptic membranes, and intracellular organelles, for example, the spine apparatus, which interacts with receptors in the membrane in dlPFC for calcium-mediated calcium release (Arnsten et al., 2021b; Datta et al., 2024). Pre-embedding immunoEM, however, likely undersamples from the PSD (Petralia and Wang, 2021). Here, we have used pre-embedding immunoEM and quantitative analyses to compare the distribution of NMDAR-GluN2B membrane expression across the macaque SGC and dlPFC.

Methods

Experimental design

This study was designed to assess the subcellular location of NMDAR-GluN2B in pyramidal and inhibitory neurons of layer III in dlPFC and SGC. Using pre-embedding immunoEM, we have labeled the NMDAR-GluN2B with immunogold particles in dlPFC and SGC. We have cut ultrathin sections, and we have performed systematic sampling using high-resolution electron microscopy within the antibody penetration zone. We analyzed all immunogold particles to determine the identity of their parent structure, and their location within that structure, to determine whether there were detectable differences in the membrane distribution of these particles between the dlPFC and SGC. To determine whether there were differences in NMDAR-GluN2B expression across types of inhibitory neurons, we performed multilabel immunofluorescence (MLIF) for the calcium-binding proteins (CBP), such as parvalbumin (PV), calbindin (CB), and calretinin (CR), in addition to NMDAR-GluN2B, and analyzed the NMDAR-GluN2B expression across CBP type using QuPath.

Subjects and tissue selection

The research was conducted with the approval of the Yale University IACUC under NIH and USDA guidelines. Tissue from the dlPFC and SGC blocks of two young adult (aged 8 and 10 years, female) macaques were used in this study. These subjects were breeding females

and were not subjected to any additional experimental procedures to our knowledge. Subjects were deeply anesthetized and underwent transcardial perfusion with 0.1 M phosphate-buffered saline (PBS), followed by 4% paraformaldehyde and 0.05% glutaraldehyde in 0.1 M PBS. Brains were removed and cut into blocks, including the dlPFC and SGC. The blocks were cut on a vibratome (Leica, Norcross, GA, USA) at a thickness of 60 μm . Free-floating sections underwent cryoprotection in ascending concentrations of sucrose (JT Baker, cat #4072-01) solution (10, 20, and 30% in PBS, each overnight) and then rapidly frozen in liquid nitrogen for long-term storage at -80°C . The sections were selected from the dlPFC block along the principal sulcus in area 46, mostly, anterior to the start of the arcuate sulcus. Tissue was selected from the SGC block along the anterior to posterior breadth of area 25 as long as the corpus callosum was in the plane.

Primary antibodies used for immunohistochemistry

To label NMDAR-GluN2B, we used the Alomone polyclonal rabbit anti-NMDAR2B antibody at 1:100 (Alomone, cat# AGC-003, RRID:AB_2040028). This antibody has been used for MLIF in various tissues, such as cultured rat neurons (Schweitzer et al., 2017), human-induced pluripotent stem cell-derived neurons (Telezhkin et al., 2016), and *in situ* macaque dlPFC (Datta et al., 2024). This antibody binds to an antigen site corresponding to amino acid residues 323–337 of the rat NMDAR2B on the extracellular N-terminus. While an antibody test in conditional or full NMDA-GluN2B knockout animals is preferable as a negative control, we were unsuccessful in locating such a test using this antibody. We performed a preadsorption control using the Alomone NMDAR-GluN2B blocking peptide (cat #BLP-GC003, Supplementary Figures S6A,B) and observed negligible labeling, suggesting that the regions outside the paratope of the antibody have minimal interactions in our tissue. In the dlPFC and SGC of each case, we further assessed the specificity of antibody labeling by measuring the percent of immunogold particles found inside mitochondria, which we deemed as non-specific labeling. This percent of immunogold particles found within mitochondrial boundaries ranged from 0.2 to 0.7%. This was much smaller than the surface area per section occupied by mitochondria, which ranged from 6 to 8%, suggesting that stochastic binding of the antibody was quite low.

To label the CBPs, we used Swant mouse monoclonal antibodies at 1:2000 (Swant guinea pig anti-PV cat# GP72 RRID:AB_2665495, mouse anti-CB-D28k cat# 300 RRID:AB_10000347, and goat anti-calretinin cat# CG1 RRID: AB_10000342, respectively), which have been widely used in macaque tissue (e.g., Joyce et al., 2020; Tsolias and Medalla, 2021; Medalla et al., 2023). To label microtubule-associated protein-2 (MAP2), we used a chicken anti-MAP2 at 1:1000 (Abcam, cat# AB5392), which has been used previously in macaque tissue as well (Tsolias and Medalla, 2021).

Immunohistochemical procedures for electron microscopy

Single-label gold immunoEM for NMDAR-GluN2B

Free-floating sections from dlPFC and SGC underwent antigen retrieval in 10 mM sodium citrate (J.T. Baker cat# 3646-01) at $30\text{--}35^{\circ}\text{C}$

for 15 min and then were cooled for another 15 min, followed by a 1-h incubation in 50 mM glycine (Sigma, cat# G-7126, in PBS). We then performed a blocking step in a solution of 5% bovine serum albumin (BSA, Jackson ImmunoResearch, cat# 001-000-162), 10% normal goat serum (NGS, Jackson ImmunoResearch cat# 005-000-121), 0.4% Triton X-100, 0.1% acetylated bovine serum albumin (BSA-c, Aurion, Electron Microscopy Sciences, cat#25557) in 0.1 M phosphate buffer (PB) for 1 h. Sections were then incubated for 72 h at 4°C in the rabbit primary antibody for NMDAR-GluN2B at 1:100 in antibody dilution buffer, which was composed of 1% BSA; 1% NGS; 0.1% BSA-c; and 0.1% Aurion coldwater fish gelatin (CWFG Electron Microscopy Sciences cat# 25560) in PB. Sections were then incubated in Aurion F(ab) fragment of goat anti-rabbit ultrasmall gold at 1:50 (Electron Microscopy Sciences, cat#25361) at 4°C overnight. Then, the sections underwent a 4% paraformaldehyde (in PBS) postfix for 5 min, followed by a 10-min incubation in 50 mM glycine, and then a few quick distilled water washes. Silver enhancement was performed using the Nanoprobes HQ Silver Kit (cat# 2012-45ML) in the dark for 20–30 min, and produced variable-sized particles. A control section was run in tandem, with the sole difference being the omission of the primary antibody from the antibody dilution buffer. When the control section was imaged, gold particles were extremely rare, even at the very edge of the tissue where labeling is typically dense and noisy, indicating that the secondary antibody was highly specific for the primary antibody (Supplementary Figures S6C,D).

Double-label immunoEM for NMDAR-GluN2B and MAP2

To perform double-labeling for NMDAR-GluN2B and MAP2, we paired NMDAR-GluN2B immunogold with immunoperoxidase non-nickel diaminobenzidine (DAB) for MAP2. We performed the antigen retrieval and glycine incubation as above. Then, sections underwent a 30-min incubation in 0.3% hydrogen peroxide at 4°C and avidin–biotin blocking (Vector cat# SP-2001) to prevent non-specific labeling by the immunoperoxidase product. Then, the sections were preblocked as above, and incubated in the primary antibody for MAP2 for 48 h at 4°C . They were then washed and incubated with biotinylated goat anti-chicken (Jackson ImmunoResearch, cat# 103-065-155) at 1:200 for 3 h at room temperature. The sections then underwent incubation with avidin–biotin complex (ABC, Vector cat# PK-6100) for 1.5 h and visualized using a DAB kit (Vector cat# SK-4100, nickel excluded). Following that, we performed washes and followed the procedures for single-label immunogold labeling as above for the NMDAR-GluN2B-gold. Initially, we tried reversing the order of operations, with the immunogold first, followed by the immunoperoxidase, and found that the gold particles fared better when performed as the second step.

EM processing

After immunolabeling, sections were processed for electron microscopy. They were post-fixed in 4% paraformaldehyde in 0.1 M PBS for 20 min and then immersed in 1% osmium tetroxide in PB, which was then immediately diluted to 0.5%, and the sections incubated in the dark for 30 min at 4°C . Then, following PB washes, sections were washed in $3 \times 5\text{--}10$ min sets of washes in ascending 50 and 70% ethanol dehydration steps, before being incubated in 1% uranyl acetate in 70% ethanol for 40 min. Sections were further dehydrated in 3×5 min 95 and 100% ethanols, followed by propylene

oxide washes (Electron Microscopy Sciences cat#20401). Finally, sections were infiltrated with Durcupan resin (Electron Microscopy Sciences cat#14040) and baked at 60°C for 72 h sandwiched between sheets of Aclar (Electron Microscopy Sciences, cat# 50425).

Immunohistochemical procedures for multi-label immunofluorescence

To label NMDAR-GluN2B and the CBPs, such as PV, CB, and CR, we performed antigen retrieval on free-floating sections, as above, except at 75–80°C, and doubled the time for the water bath and cooling steps. We then performed the glycine and blocking steps, as above. The antibody dilution buffer was the same as above, but excluding the CWFG and substituting normal donkey serum (Jackson ImmunoResearch, cat# 017-000-121). Primary incubation occurred in antibody dilution buffer for NMDAR-GluN2B, PV, CB, and CR for 72 h at 4°C. Then, we incubated the sections in species-specific AlexaFluor donkey secondary antibodies at 1:100 (Invitrogen, AlexaFluor-568 anti-mouse cat# A10037, AlexaFluor-488 anti-rabbit cat# A32790, and AlexaFluor405 anti-goat cat# A48259) and a biotinylated donkey anti-guinea pig (Jackson ImmunoResearch cat# 705-065-148) for 3 h at 4°C in the dark. Then, sections were washed and incubated in Streptavidin-647 (Invitrogen, cat# S21374) at 1:200 for 3 h at room temperature. Sections were mounted using ProLong Gold Antifade Mountant (Invitrogen, cat# P36930). We also ran a preadsorption control test for NMDAR-GluN2B. One section was run in tandem with the above, but incubated in antibody dilution buffer containing the Alomone NMDAR-GluN2B primary antibody, but with the addition of the blocking peptide for the NMDAR-GluN2B antigen (Alomone, cat# BLP-GC003), at 10x the concentration of the primary antibody (Supplementary Figures S6A,B). The sections were incubated in a goat anti-rabbit Alexafluor secondary antibody (Invitrogen, cat# A11008).

Imaging procedures, 2D sampling, and analysis for immunoEM

Imaging and sampling

Two or more sections were processed per animal per area for single-labeled NMDAR-GluN2B analysis and for the double-labeling MAP2/NMDAR-GluN2B analysis. For the single-label NMDAR-GluN2B analysis, a minimum of four blocks, two from each section, were examined per area per subject for sampling. One block per section per area was analyzed for the double-labeled MAP2/NMDAR-GluN2B analysis. Blocks were dissected from layer III within the principal sulcus of the dlPFC (area 46) and, along the medial wall of the SGC (area 25), mounted on Durcupan resin blocks and then sectioned at 50 nm on an ultramicrotome (Leica). Short series (10–20 sections, typically) were collected on Butvar-coated (Electron Microscopy Sciences, cat# 11860) copper slot grids near the top of the section. Grids were imaged using a Talos L120C transmission electron microscope (Thermo Fisher Scientific) coupled with a Ceta CMOS camera. We mapped each section and outlined the boundaries of the antibody penetration region, which is typically reliable within 5–20 µm from the edge of the tissue section but can be variable by section depending on the plane of cut. Using a meander-scan approach, we used a systematic sampling acquisition

protocol, snapping every second or third field of view (depending on the extent of the antibody penetration zone) as we traversed the antibody penetration zone of the section, at 11–13,000x magnification. For single-labeled NMDAR-GluN2B immunogold sections, approximately 300–475 images were sampled per cortical area per subject, depending on immunolabeling density (Monkey 1: SGC, 293 images, dlPFC, 475 images; Monkey 2: SGC, 305 images, dlPFC 346 images). For double-labeled MAP2/NMDAR-GluN2B sections, approximately 200–500 images were acquired for analysis per area per case, depending on immunolabeling density (Monkey 1: SGC, 203 images, dlPFC, 289 images; Monkey 2: SGC, 550 images, dlPFC, 292 images). Images were adjusted for brightness and contrast using Adobe Photoshop CS5 Extended (version 12.0.4 × 64, Adobe Systems Incorporated) for figures.

Analysis of 2D sampled electron micrographs

All 2D images were analyzed using Reconstruct (Fiala, 2005). We examined all gold particles in all images and classified each particle's parent structure as a spine, axon, bouton, dendrite, likely glial process, cell soma, or undetermined structure using classical criteria (Peters et al., 1991). Likely because of differences in fixation conditions between the subjects, the total proportion of undetermined structures was variable across subjects, in particular for small or broken structures, or for thin structures with mitochondria that did not have synaptic interactions, spines, or telltale indicators of axonal, glial, or dendritic identity. We classified immunogold particles as cytoplasmic if not touching any external membranes, and synaptic if found touching the post-synaptic density (PSD) of a synapse. We classified immunogold particles as perisynaptic if the immunogold particle was within approximately <100 nm from the synapse along the membrane, and extrasynaptic if the immunogold particle was >100 nm from the PSD along the membrane (Hardingham and Bading, 2010; Petralia et al., 2010) though the extent of the perisynaptic region appears to be somewhat loosely defined (Newpher and Ehlers, 2008; Gladding and Raymond, 2011). One caveat of our 2D sampling approach is that extrasynaptic NMDAR-GluN2B may truly be perisynaptic to synapses that are out of the plane of section. The total number of GluN2B+ spines sampled varied by area by case, depending on immunolabeling success and plane of sectioning (Monkey 1: SGC, 229 spines, dlPFC 483 spines; Monkey 2: SGC, 242 spines, dlPFC 162 spines). After tracing the outline of each spine head containing positive NMDAR-GluN2B immunolabeling, we computed the major Feret's diameter of each spine to determine whether there were detectable differences in NMDAR-GluN2B+ spine head size across cortical areas. To determine whether we could detect differences across randomly sampled NMDAR-GluN2B-negative spine heads across areas, we selected one image sampling session from each cortical area per subject and measured all spines present that were not NMDAR-GluN2B+, which we call "neuropil" spines for comparison to NMDAR-GluN2B+ spines. Given that we performed only a 2D analysis, it is important to note that these spines may have had NMDAR-GluN2B immunogold particles in planes outside the imaged section, and thus, the type II error rate (false negative) is elevated for this analysis, although it represents a systematic bias equivalently present across the compared cortical areas (NMDAR-GluN2B-negative spines sampled, Monkey 1: SGC, 113 spines, dlPFC 153 spines; Monkey 2: SGC, 310 spines, dlPFC 124 spines). For all membrane-bound immunogold particles in spines, we measured the shortest distance from the membrane to the smooth

endoplasmic reticulum (SER) spine apparatus in the plane, making multiple measurements from the site of gold contact with the membrane and the closest elements of the SER in the plane. Given that there may be elements of the SER outside the sectioning plane that may have been actually closer to the immunogold particles (e.g., just above or below), this analysis may also contain an elevated type II error rate.

Imaging procedures, sampling, and analysis for MLIF

Imaging and sampling

Sections were imaged on a Zeiss LSM 880 Airyscan with the Plan-Apochromat 20x/0.8 M27 objective. Z-stacks were obtained with $\sim 1\text{-}\mu\text{m}$ steps through the depth of the tissue under laser excitation at 405 nm, 488 nm, 561 nm, or 633 nm. Emission filter bandwidths and sequential scanning acquisition were set up in order to avoid spectral overlap between fluorophores. Confocal images were deconvolved with Huygens Professional version 22.04 (Scientific Volume Imaging, The Netherlands) using uniform parameters. For quantitative analysis in the dlPFC, we located the principal sulcus and used the NMDAR-GluN2B labeling in pyramidal neurons, and the distribution of inhibitory neurons, which differentially populate laminar compartments (Joyce et al., 2020; Medalla et al., 2023) to locate layer III. In two sections per cortical area per case, we systematically sampled from deep layer III in parallel to layer I, acquiring a z-stack in every other field of view in dlPFC area 46 along the axis of the principal sulcus. We exhaustively sampled the medial wall of SGC area 25, given its shorter breadth, and used similar metrics as in the dlPFC to locate layer III. From each stack, we extracted a ministack of a few optical sections, typically less than five, from the top of the stack, and then again from the bottom of the stack, ensuring no cells were present in both, and discarding the very top or bottom optical section of the stack, given that they can contain higher background labeling. We obtained maximum intensity projections from these mini-stacks for quantitative analysis (Monkey 1: SGC, 12 images; dlPFC, 17 images; Monkey 2, SGC, 17 images; dlPFC, 15 images) using QuPath 0.5.0 (Bankhead et al., 2017). If the images did not have uniform illumination, we analyzed the image in parts containing uniform illumination.

Analysis

To perform our quantitative analysis, we manually segmented the PV, CB, and CR inhibitory neurons. We also segmented CB+ pyramidal neurons (Kondo et al., 1999; Joyce et al., 2020; Datta et al., 2024) for our analysis (“CB pyrs”), given that these are prominent in the superficial layers of the prefrontal cortex, with a high density in SGC (Joyce et al., 2020), and these neurons are selectively vulnerable to loss in Alzheimer’s disease (Hof and Morrison, 1991). These neurons are identifiable by their faint CB labeling and morphological attributes consistent with pyramidal neurons, namely a pyramidal-shaped soma and apical dendrite oriented toward layer I. In the isolated NMDAR-GluN2B channel, we traced neurons that were clearly pyramidal, given that we wanted to avoid any CBP-negative cells positive for NMDAR that could be glial cells, CBP-negative inhibitory neurons, or excitatory interneurons impinging from nearby layer IV. Pyramidal neurons were identified using morphological criteria, namely a pyramidal-shaped soma and thick apical dendrite oriented toward layer I; however, variability in the sectioning plane for each block introduced some variability in the number of positively identified pyramidal neurons that could be obtained

in each area because a cutting plane not aligned to the orientation of the pyramidal neurons could occlude some of the apical dendrite labeling (e.g., for apical dendrites traveling “through” the plane of section). Some of these “N2B pyrs” also had faint CB labeling, so there is some overlap of cells between the “N2B pyrs” and the “CB pyrs” categories. We also sampled from immunonegative “neuropil” segments of tissue containing no obviously labeled processes, for “background” calibration. We measured the mean intensity (MI) using $0.1\text{-}\mu\text{m}$ pixel size for all NMDAR-GluN2B+ pyramidal neuron traces, including those that were also faintly CB+, and neuropil regions. Then, we averaged the MI across immunonegative background regions and across the NMDAR-GluN2B+ pyramidal neurons. We then used these numbers to create an index for binning all CBP+ inhibitory neurons. We deemed a CBP+ neuron NMDAR-GluN2B negative if it had an MI at or below the average across sampled background regions and NMDAR-GluN2B strong if it had an MI at or above the mean across NMDAR-GluN2B+ pyramidal neurons (including pyramidal neurons also faintly positive for CB), and included a few intermediate bins (“weak” or “moderate”). We then averaged the proportion falling into each bin across cases. See [Supplementary Figure S5](#) for these data by case and area and [Supplementary Figures S5C–F](#) for the bin calibration for each area and case (left side of plots). Total numbers of neurons were variable across areas (Monkey 1: SGC, 383 CBP+ inhibitory neurons and 719 CB/NMDAR-GluN2B+ pyramidal neurons, dlPFC, 452 CBP+ inhibitory neurons, 254 CB/NMDAR-GluN2B+ pyramidal neurons; Monkey 2: SGC, 864 CBP+ inhibitory neurons and 834 CB/NMDAR-GluN2B+ pyramidal neurons, dlPFC, 449 CBP+ inhibitory neurons, 97 CB/NMDAR-GluN2B+ pyramidal neurons) given that these cortical areas have variable densities of these inhibitory neurons as previously quantified (Joyce et al., 2020). Images were adjusted for brightness and contrast using Adobe Photoshop CS5 Extended (version 12.0.4 \times 64, Adobe Systems Incorporated) for figures.

Statistical analysis

Statistical analysis and plot preparation for figures were performed in Prism (GraphPad) and SPSS (IBM). We assessed the properties of our distributions and determined the appropriate parametric or non-parametric tests. To analyze the membrane distribution of NMDAR-GluN2B particles, average spine sizes, and distances of immunogold particles to the SER, we averaged across Monkey 1 and Monkey 2 and performed one-way ANOVAs with *post-hoc* Tukey’s tests for pairwise comparison. To analyze the NMDAR-GluN2B expression bins across inhibitory neuron somata, we used a three-way ANOVA with *post hoc* Bonferroni adjustments for pairwise comparisons. Figures were prepared in Adobe Illustrator 25.0.1 (Adobe Systems Incorporated version 27.7).

Results

NMDAR-GluN2B is more frequently synaptic in dlPFC spines and extrasynaptic in SGC spines

To study the membrane localization of NMDAR-GluN2B in SGC and dlPFC, we used pre-embedding immunoEM to label NMDAR-GluN2B with immunogold particles and performed systematic 2D sampling in layer III of the SGC and dlPFC. Spines found in layer III of

both areas were frequently NMDAR-GluN2B+ using both post-embedding and pre-embedding techniques (Figures 1, 2). In our pre-embedding preparation (Figure 2 and Supplementary Figure S1), we most often found NMDAR-GluN2B immunolabeled particles in the cytoplasm, which we have interpreted as intracellular trafficking events. Synaptic NMDAR-GluN2B was readily observable in SGC and dLPFC spines (Figures 2A1,B1,B2; Supplementary Figures S1A,E). We also observed NMDAR-GluN2B in membranes outside the synapse at extrasynaptic and perisynaptic locations (Figures 2A2,A3,B3; Supplementary Figures S1B–D,F–H). We pooled the data from all spines within each cortical area per monkey and quantified the proportion of NMDAR-GluN2B immunogold particles found at synaptic, perisynaptic, extrasynaptic, and cytoplasmic locations (Figure 2C). Figure 2C demonstrates that the SGC in both monkeys had a higher ratio of extrasynaptic-to-synaptic immunogold particle expression of NMDAR-GluN2B in spines (~2:1), while NMDAR-GluN2B immunogold particles in dLPFC spines were closer to equally likely to be found in the synapse than at extrasynaptic sites (synaptic-to-extrasynaptic ~1:0.9). Figure 2D shows that when membrane-bound immunogold particle patterns are averaged across areas and subjects, thus excluding the substantial expression of cytosolic particles, these relationships were significant, indicating that NMDAR-GluN2B were more likely to be found at extrasynaptic sites in SGC spines than in dLPFC spines.

We also performed supplemental analyses to characterize the spines that expressed NMDAR-GluN2B. We measured the major Feret's diameter of each NMDAR-GluN2B+ spine, and in a smaller set of sampled images per subject and cortical area, we also measured all other NMDAR-GluN2B-spines present in the images (Supplementary Figure S2A). The mean major diameter of NMDAR-GluN2B+ spines across the two cortical areas was similar, approximately ~0.6 μm . The mean diameter of NMDAR-GluN2B+ spines was larger for both animals than were NMDAR-GluN2B-spines (Supplementary Figure S2), though when the cases were averaged only the difference in the SGC was significant (Supplementary Figure S2), with the caveat that some NMDAR-GluN2B-spines may contain NMDAR-GluN2B in planes above or below the plane sampled in our

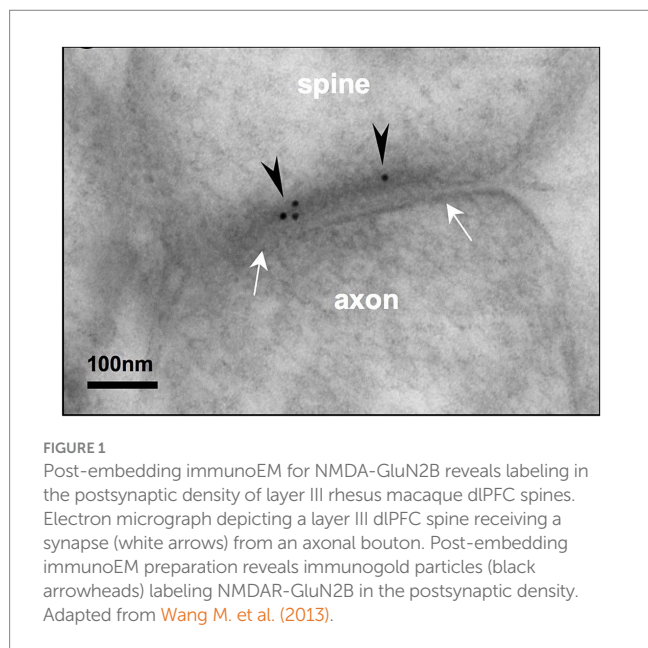
analysis. We also measured the distance of each membrane-bound NMDAR-GluN2B immunogold particle to any evident SER spine apparatus in the plane. Many NMDAR-GluN2B were within tens of nanometers from the SER, indicating that they are within physiological range to evoke calcium-mediated calcium release from the SER (Supplementary Figure S2B) as demonstrated in other systems (see Datta et al., 2024). Given the constraints of our 2D sampling paradigm, many of these membrane-bound NMDAR-GluN2B immunogold particles may be closer to SER elements that were present in unsampled portions of the spine above and below the plane of the section. We also observed presynaptic NMDAR-GluN2B labeling (Supplementary Figure S3), although these gold particles were very rarely adhered to the membrane (<5% immunogold particles found in NMDAR-GluN2B+ boutons sampled in both dLPFC and SGC). They were mostly found in the cytoplasm amid the vesicles.

NMDAR-GluN2B is more likely to be extrasynaptic in SGC than dLPFC putative excitatory dendrites

In addition to spines, we also characterized NMDAR-GluN2B expression in dendritic shafts that were contained in our sampled images. We were able to identify some dendrites that had spines in plane, indicating they were likely the dendrites of excitatory neurons (Figures 3A2–B1), given that cortical excitatory neurons are spiny (Peters et al., 1991; Hsu et al., 2017). To supplement this analysis, we then turned to double-label immunoEM to evaluate excitatory dendritic shafts, using NMDAR-GluN2B and MAP2, a protein prominently expressed in the dendrites of pyramidal neurons in monkey PFC (e.g., Tsolias and Medalla, 2021), although we have recently observed that MAP2 can be expressed in proximal dendrites of inhibitory neurons in dLPFC (Joyce et al., 2024a). We then performed systematic sampling in tissue double-labeled for MAP2 and NMDAR-GluN2B. In MAP2+ dendrites, synapses formed on dendritic shafts were rare, and in only one instance, we observed a MAP2+ dendrite containing more than one synapse on the dendritic shaft in the plane, indicating that it may have been an inhibitory dendrite. Given that the majority of asymmetric presumed excitatory synapses formed on prefrontal pyramidal neurons occur on spines rather than dendritic shafts (Hsu et al., 2017), the rarity of dendritic shaft synapses found in our sampled MAP2+ dendrites suggests that the majority of them were likely excitatory dendrites. Among MAP2+ dendrites (e.g., Figures 3A1,B2; Supplementary Figure S4), we counted the gold particles and quantified their location (Figure 3C; Supplementary Figure S4). In SGC, NMDAR-GluN2B was more frequently found in the membranes of dendritic shafts than in dLPFC, and this relationship was significant (Figure 3D; Supplementary Figure S4). Synaptic NMDAR-GluN2B in MAP2+ dendritic shafts were exceedingly rare (<0.2% of all immunogold NMDAR-GluN2B for both areas and cases).

Somatic extrasynaptic NMDAR-GluN2B expression

Membrane expression of NMDAR-GluN2B at the soma occurred in both SGC and the dLPFC, though this was difficult to quantify because cell identity was not always determinable in our 2D sampled images. In one SGC section, we found pyramidal-like soma with an



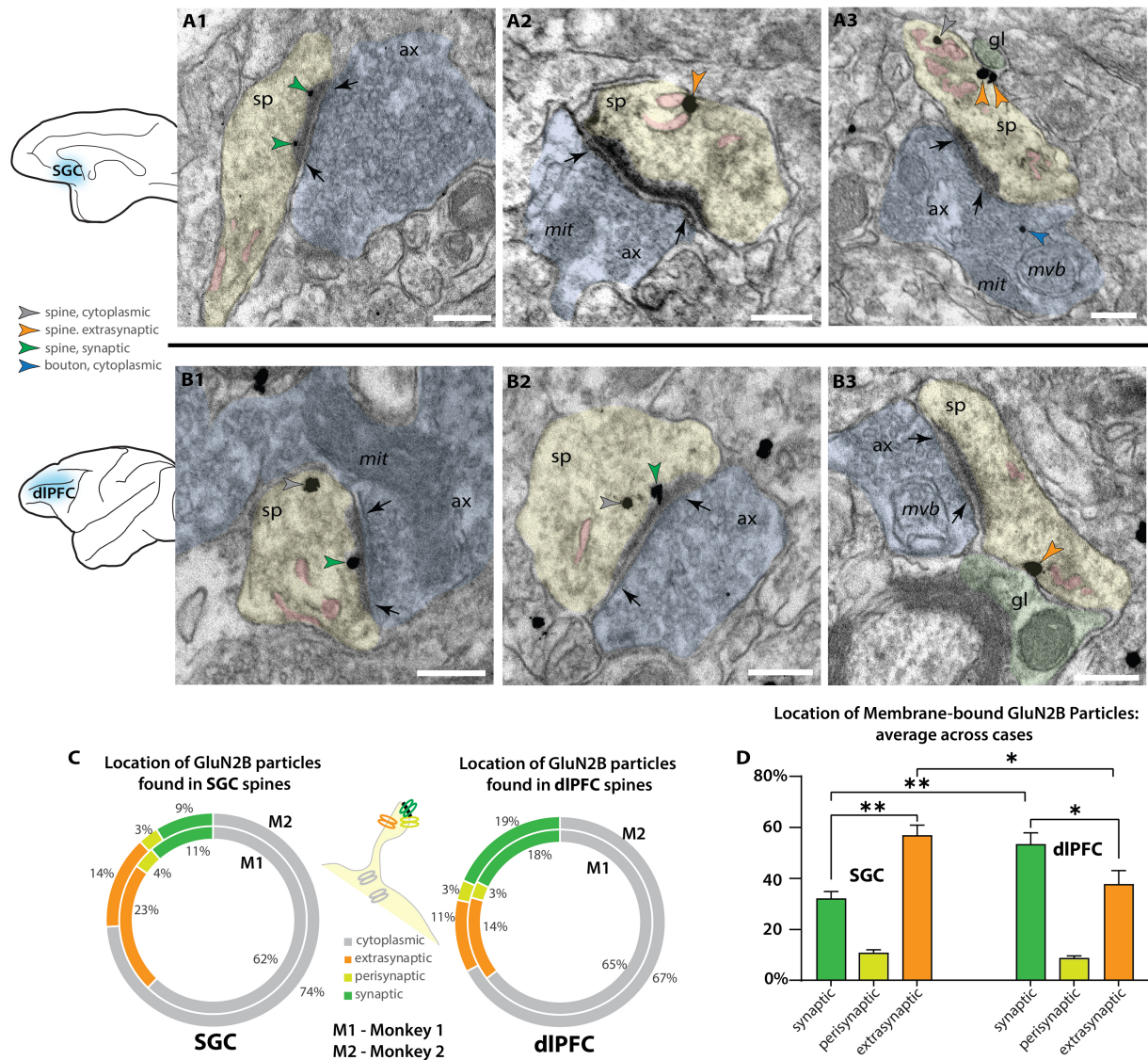


FIGURE 2

Higher proportion of extrasynaptic GluN2B immunogold particles in layer III SGC spines than dIPFC spines. (A) Electron micrograph depicting spines in SGC layer III. (A1) An SGC spine (sp, pseudocolored yellow) with NMDAR-GluN2B immunogold particles (green arrowheads) in the postsynaptic density of a synapse (black arrows) formed by an axonal bouton (ax, pseudocolored blue). The spine contains a spine apparatus, an extension of the smooth endoplasmic reticulum (SER, pseudocolored pink) in the spine neck. (A2,A3) SGC spines with NMDAR-GluN2B appearing adhered to extrasynaptic membranes (orange arrowheads), near the SER. In A3, the extrasynaptic NMDAR-GluN2B is apposed to a structure consistent with glial morphology (gl, pseudocolored green), and the bouton contains a presynaptic cytoplasmic NMDAR-GluN2B (blue arrowhead) among the vesicles. (B) Electron micrographs depicting spines in dIPFC layer III. (B1,B2) dIPFC spines containing synaptic NMDAR-GluN2B (green arrowheads), and cytosolic NMDAR-GluN2B (gray arrowheads), which are likely being trafficked. (B3) A dIPFC spine with an extrasynaptic NMDAR-GluN2B in the spine neck, apposed to a structure consistent with glial morphology, and near a spine apparatus. (C) Nested pie charts depicting the location of NMDAR-GluN2B immunogold particles found in the cytoplasm (gray), post-synaptic density (green), perisynaptic membrane (yellow-green), and extrasynaptic membrane (orange) of NMDAR-GluN2B+ spines. (D) Plot depicting the location of membrane-bound NMDAR-GluN2B immunogold particles, in relation to the synapse, averaged across M1 and M2. Error bars depict standard deviation. One-way ANOVA, $F(5,6) = 67.71$, $p < 0.001$, with *post-hoc* Tukey's test. * $p < 0.05$; ** $p < 0.01$, *** $p < 0.001$; **** $p < 0.0001$; scale bars, 200 nm. ax, axon; gl, glial process; mit, mitochondria; mvb, multivesicular body; SER, smooth endoplasmic reticulum spine apparatus; sp, spine.

apical dendrite, basal dendrite, and axon initial segment well contained within the antibody penetration zone. The pyramidal-like neuron had robust NMDAR-GluN2B labeling in the cytoplasm of the soma and proximal dendrites and at extrasynaptic sites (Figure 4), in contrast to sparser NMDAR-GluN2B labeling in surrounding neuropil (Figure 4H). In particular, we observed robust NMDAR-GluN2B in the nucleus and the nuclear membrane (Figure 4H).

High-likelihood inhibitory dendrites have less synaptic NMDAR-GluN2B expression than spines, as well as extrasynaptic expression

We also examined the expression of NMDAR-GluN2B in putative inhibitory dendrites. Inhibitory dendrites in the cortex are

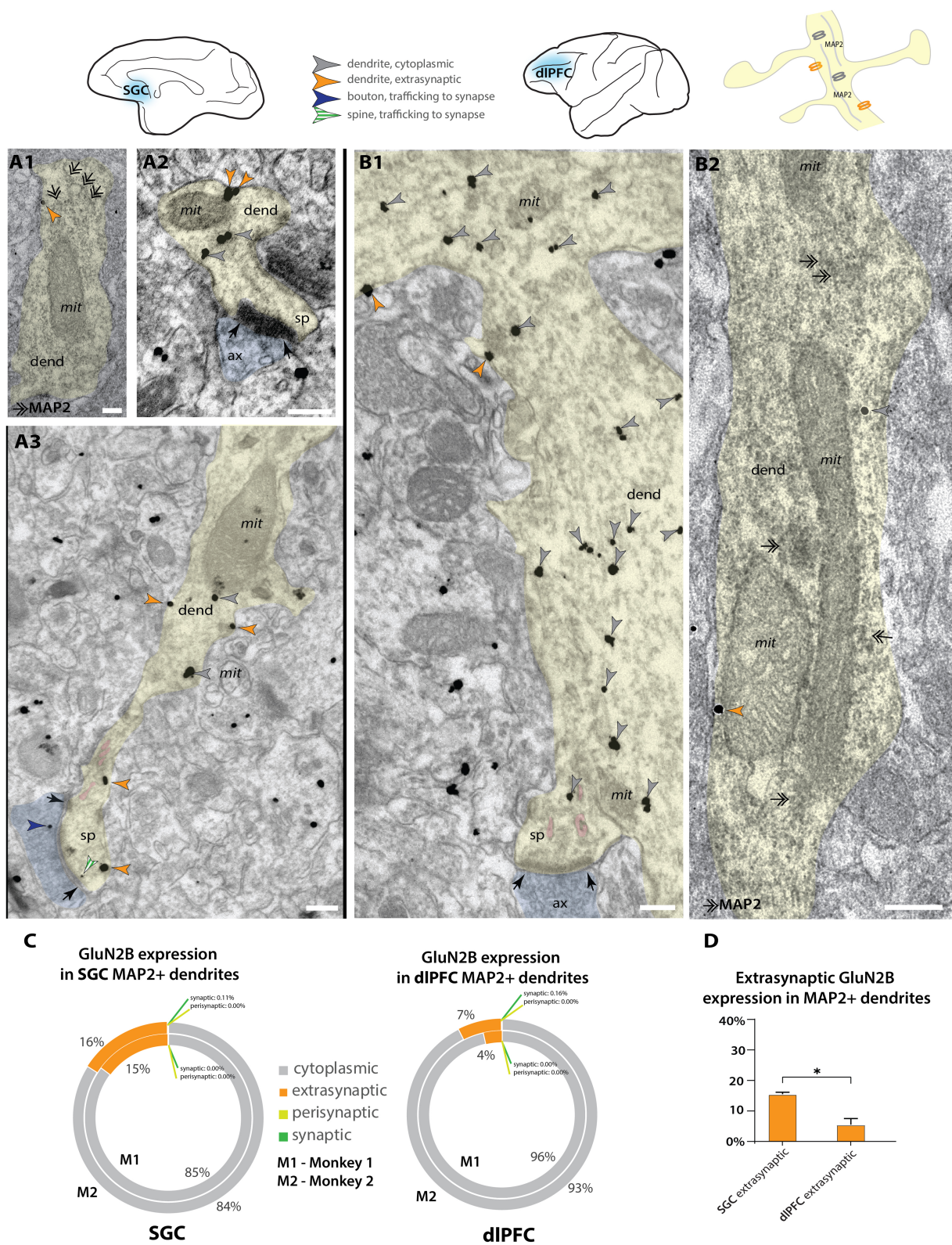


FIGURE 3

Higher extrasynaptic expression in dendrites of putative excitatory neurons of SGC than dIPFC. (A) Electron micrographs from layer III SGC. (A1) A putative excitatory dendrite, labeled with MAP2+ non-nickel immunoperoxidase diaminobenzidine (smudge-like precipitate, double-headed arrows), expressing an extrasynaptic NMDAR-GluN2B (orange arrowhead); (A2,A3) NMDAR-GluN2B at extrasynaptic (orange arrowheads), cytoplasmic (gray arrowheads), or near-synaptic locations (gray-white striped arrowhead) in putative excitatory dendrites. (B) Electron micrographs from layer III dIPFC. (B1) A putative excitatory dendrite, with a spine in plane, expressing cytoplasmic and extrasynaptic NMDAR-GluN2B. (B2) A putative excitatory dendrite, labeled with MAP2, expressing extrasynaptic and cytoplasmic NMDAR-GluN2B. (C) Nested pie charts depicting the percent of NMDAR-GluN2B

(Continued)

FIGURE 3 (Continued)

immunogold particles found at cytoplasmic, extrasynaptic, perisynaptic, and synaptic locations in MAP2+ dendritic shafts in SGC (left) and dlPFC (right) of Monkey 1 (inside) and Monkey 2 (outside). Synapses on the shaft of MAP2+ dendrites were rare, and synaptic NMDAR-GluN2B on MAP2+ shaft synapses was extremely rare (<0.2% of all immunogold particles in all areas analyzed). (D) Mean percent of extrasynaptic NMDAR-GluN2B immunogold particles across all MAP2+ dendrites in SGC and dlPFC. One-way ANOVA with *post-hoc* Tukey's test, $F(3,4) = 1,691$, $p < 0.0001$. * $p < 0.05$; pink pseudocolor, SER spine apparatus; black arrows, synapse; scale bars, 200 nm; ax, axon; dend, dendrite; MAP2, microtubule-associated protein-2; mit, mitochondria; sp, spine.

predominantly aspiny or sparsely spiny and receive most synaptic input on the dendritic shaft (Peters et al., 1991). We classified inhibitory dendrites as “high likelihood” based on the presence of two or more shaft synapses in the plane, and no spines in the plane. Figures 5A,B depicts examples of these dendrites in SGC and dlPFC. NMDAR-GluN2B found in the postsynaptic density (Figure 5C, 1–3% across areas) occurred at a much lower frequency than in spines found in the same sampled images (~10% synaptic NMDAR-GluN2B in SGC spines vs. ~20% in dlPFC, Figure 2C). In both areas, the extrasynaptic proportion was slightly above 10%, and there were no differences detected across areas when the subjects were pooled. When NMDAR-GluN2B was found in the PSD, the immunogold particles were most often affiliated with the far edge of the PSD and rarely in the main body of the synapse (e.g., Figures 5A3,B2).

NMDAR-GluN2B expression is roughly equivalent across inhibitory neuron somata in both areas

We were also interested in whether the NMDAR-GluN2B expression level varied across inhibitory neuron types. In primates, the calcium-binding proteins (CBP) are a useful way to classify inhibitory neurons. The CBPs, such as parvalbumin (PV), calbindin (CB), and calretinin (CR), label upward of 85% of all cortical inhibitory neurons and are largely non-overlapping, that is they are largely neurochemically distinct (Conde et al., 1994; DeFelipe, 1997; Medalla et al., 2023). To measure whether there were expression-level differences across neurons labeled by the CBPs, we used multilabel immunofluorescence (MLIF) for PV, CB, CR, and NMDAR-GluN2B (Figures 6A,B; Supplementary Figures S5A,B), and sampled z-stacks in layer III of SGC and dlPFC of both cases. In maximum intensity projections, we segmented traces for the somata of the inhibitory neurons. In the isolated GluN2B channel, we traced the outlines of pyramidal-like neurons and sampled immunonegative “background” regions of the tissue that contained no labeled processes. Because our MLIF did not also contain a fiduciary pyramidal neuron marker, cells were classified as “pyramidal-like” if they were negative for CR, PV, or strong CB labeling, and additionally featured a large pyramidal-shaped somata, and labeling in thick apical-like dendrites oriented toward layer I. We measured the mean intensity (MI) for each trace and then compared the MI in inhibitory neuron traces to the MI found in pyramidal neurons and in “background”-like immunonegative areas (Supplementary Figures S5C–F). This allowed us to create expression bins per sampling site, using the levels of expression in the NMDAR-GluN2B pyramidal neurons and the “background” regions to create normalized expression bins that could then be combined across sampling sites. Figures 6C,D depict the

results of this analysis (see Supplementary Figure S5 for a more detailed report). Only a small proportion of inhibitory neuron somata for each CBP category expressed NMDAR-GluN2B at an equivalent MI to the traces of neighboring pyramidal neurons (~5–15%, “N2B-strong” category, Figures 6C,D; Supplementary Figure S5G). Approximately one quarter or less of each inhibitory neuron type was negative for NMDAR-GluN2B, meaning their NMDAR-GluN2B expression level was below the average from the sampled “background” regions (“negative” category, Figures 6C,D; Supplementary Figure S5G). A three-way ANOVA revealed a significant main effect for NMDAR-GluN2B expression level $F(3,24) = 63.302$, $p < 0.001$, $\eta^2 = 88.8$, but a *post-hoc* Bonferroni-adjusted pairwise comparison revealed that the only significant difference across areas was for the CB N2B-negative category ($p = 0.012$), with, on average, 27% of dlPFC layer III CB neurons being negative for NMDAR-GluN2B, while only 7% of SGC layer III CB neurons were negative for NMDAR-GluN2B.

Discussion

The current study found variation in the synaptic vs. extrasynaptic expression of NMDAR-GluN2B in dendrites and spines of layer III of the macaque SGC and dlPFC. Our data suggest that there is a higher proportion of NMDAR-GluN2B expressed at extrasynaptic membrane locations among putative pyramidal neuron dendrites in SGC than dlPFC, while synaptic NMDAR-GluN2B were more prominent in dlPFC. As the SGC appears to be relatively enriched in NMDAR-GluN2B (Burt et al., 2018)—although this pattern may be less pronounced in rhesus macaques (Chen et al., 2023)—our data suggest that there is a substantial population of extrasynaptic NMDAR-GluN2B in SGC compared to some other regions of the PFC. The prevalence of synaptic NMDAR-GluN2B in dlPFC is consistent with previous studies demonstrating synaptic NMDAR-GluN2B in this region, and the importance of NMDAR-GluN2B to dlPFC neuronal firing during working memory (Wang M. et al., 2013). This contrasts with putative inhibitory neurons in both areas, where NMDAR-GluN2B membrane expression was rarely synaptic, with no detectable areal differences among inhibitory-like dendrites sampled in this study. When present, synaptic NMDAR-GluN2B in inhibitory neuron dendrites were found at the periphery of the PSD.

Our study utilized pre-embedding immunoEM, which entails the binding of antibodies to antigens in free-floating sections that are tens of microns in thickness, followed by processing for EM, embedding in resin, and ultramicrotomy to section into ultrathin sections for EM imaging. This is in contrast to post-embedding immunoEM, in which immunohistochemical procedures are performed on sections tens of nanometers in thickness, from blocks that have already been processed for EM and embedded in resin (e.g., Figure 1). We use

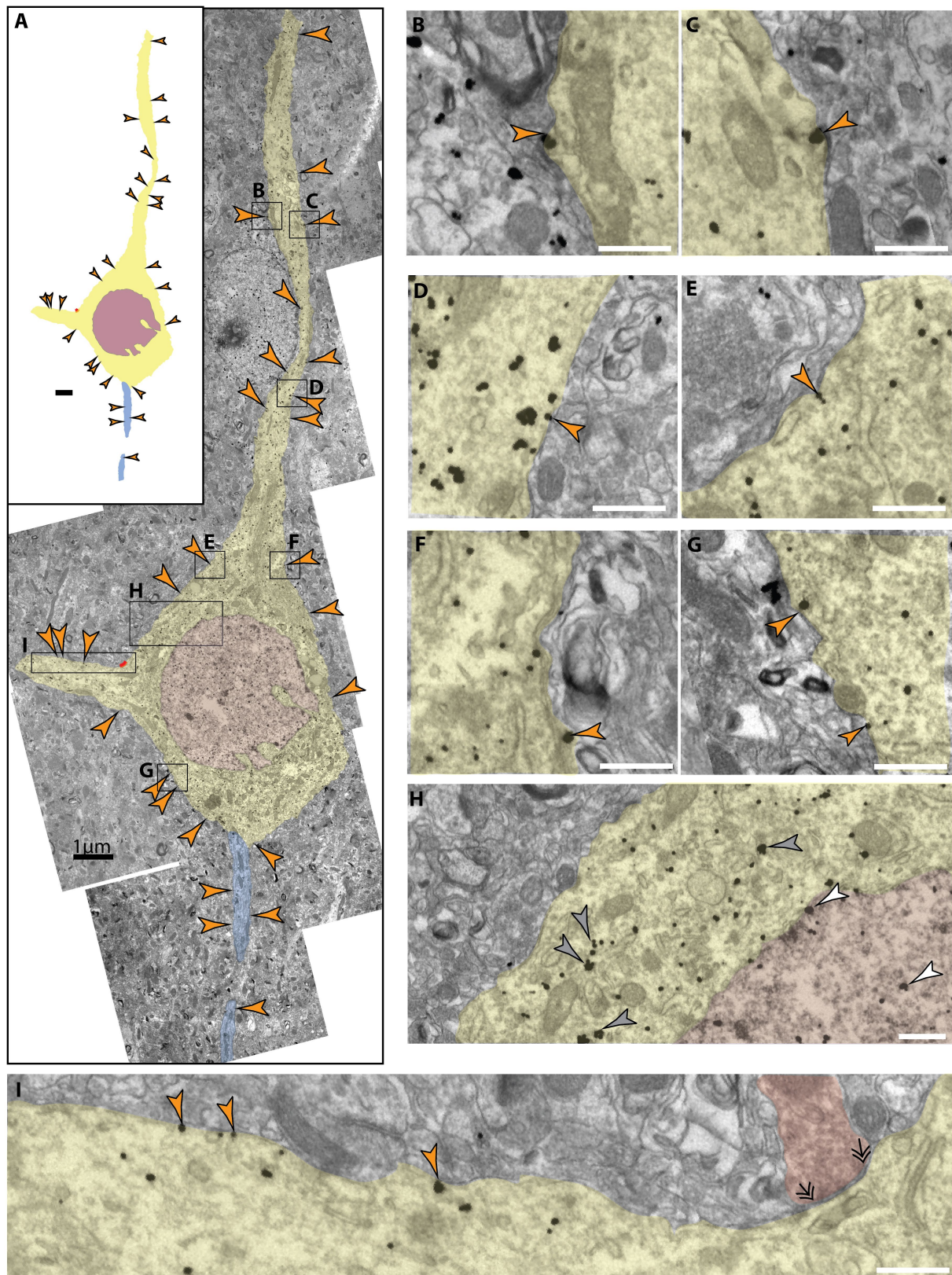


FIGURE 4
 Extrasynaptic NMDAR-GluN2B expressed at a pyramidal-like soma in layer III SGC. **(A)** A panorama of stitched electron micrographs depicting a pyramidal-like soma and dendrites (pseudocolored yellow), including the nucleus (pseudocolored plum) and its axon initial segment (pseudocolored blue). NMDAR-GluN2B is prevalently expressed in extrasynaptic membranes (orange arrowheads) at the soma and proximal processes. Black boxes depict inset locations for subsequent panels. **(B–G)** Insets from **(A)** depicting extrasynaptic NMDAR-GluN2B at higher magnification. **(H)** Inset from

(Continued)

FIGURE 4 (Continued)

(A) selected to emphasize the antibody labeling specificity of the labeled neuron compared to the surrounding neuropil as well as to emphasize nuclear labeling. Few NMDAR-GluN2B immunoparticles are evident in the surrounding neuropil, while the pyramidal-like soma densely expresses cytosolic NMDAR-GluN2B immunoparticles (gray arrowheads). NMDAR-GluN2B immunoparticles are also present in the nucleus (pseudocolored plum, white arrowhead). (I) Inset from (A) depicting several more extrasynaptic NMDAR-GluN2B on a basal dendrite as well as a symmetric synapse (double arrowheads) formed on the soma (axon pseudocolored red). Scale bars in (B–I), 200 nm.

pre-embedding immunoEM for examining molecular localization in organelles and extracellular membranes because of its gentler treatment of tissue ultrastructure, allowing the ability to access extrasynaptic compartments more readily given their preservation. However, pre-embedding immunoEM has its caveats, such as limited antibody penetration, and the difficulty of achieving full antibody access to the dense matrix of proteins in the PSD (reviewed in Petralia and Wang, 2021). For this reason, pre-embedding immunoEM likely undersamples from the PSD, a critical constraint for our study, which means that our data should not be interpreted as ground truth absolute expression data for synaptic versus extrasynaptic expression, but rather a dataset that can reveal comparative relationships between cortical areas subjected to the same labeling and analytical procedures. This methodological difference likely explains, in part, the higher NMDAR-GluN2B synaptic presence that was observed in an earlier study of dlPFC (Wang M. et al., 2013), which may be further compounded by differences in antibody performance. The critical piece of evidence that we offer is that it appears that the detectable membrane expression patterns can shift across primate PFC areas under equivalent labeling procedures, with increasing extrasynaptic expression in the SGC as compared to the dlPFC.

There are a few important caveats to consider for interpretation of our study. The first is that we utilized two female subjects, so our cohort was small and not sex-balanced. In particular, despite the limited sample size, our results were substantially consistent across the two subjects. However, our results may represent sex-specific effects that are distinct from NMDAR-GluN2B expression in the SGC and dlPFC of male subjects. There are notable sex differences in the phenotype of depression in humans and rodent models (Shansky et al., 2006; Seney and Sibille, 2014; Seney et al., 2018). Moreover, there is a higher incidence of Alzheimer's Disease in women, even when controlling for life expectancy (Aggarwal and Mielke, 2023), so future studies will be required to determine whether the patterns observed here are consistent in male subjects as well. Another important caveat is that we have only examined the membrane patterns of NMDAR-GluN2B, a subunit often linked with extrasynaptic expression (Tovar and Westbrook, 1999; Papouin et al., 2012), but other subunits may also be expressed extrasynaptically (Thomas et al., 2006; Harris and Pettit, 2007; Kortus et al., 2023), and a thorough study of the membrane expression patterns of NMDAR-GluN2A, -GluN2C, and -GluN2D across diverse cell types will form a much more complete picture of the patterns of synaptic and extrasynaptic NMDAR across heterogeneous PFC regions.

Extrasynaptic NMDARs likely serve important functions in normal homeostatic physiological conditions. For example, studies in rodent hippocampal cultures and *ex vivo* slice preparations suggest that extrasynaptic NMDARs are stored for shuttling and trafficking in and out of synapses, even for those NMDARs that are outside the loosely defined perisynaptic region (Kortus et al., 2023; reviewed in Groc and Choquet, 2020; Petit-Pedrol and Groc, 2021). Extrasynaptic

NMDARs can propagate dendritic spikes after an initial depolarizing event according to early theoretical modeling (Rhodes, 2006) and more recent slice electrophysiology studies in rodents, e.g., the mPFC (Chalifoux and Carter, 2011) and human medial temporal cortex (Testa-Silva et al., 2022). Dendritic NMDA spikes play a role in integrative processes and signal amplification *in vivo* in mouse somatosensory cortex (Palmer et al., 2014). Extrasynaptic NMDARs have also been linked with astrocytic glutamate release, producing slow synchronous events which could be involved in homeostatic regulation of neuronal assemblies, according to studies in rodent thalamic *ex vivo* slice preparations (Parri et al., 2001), rodent hippocampus slices (Bezzi et al., 2004; Fellin et al., 2004), and *in vivo* mouse neocortex (Poskanzer and Yuste, 2016). Furthermore, recent studies have suggested that conformational changes in the intracellular c-terminal domain of NMDAR may induce metabotropic-like signaling events in the absence of ionotropic functions, for example, inducing long-term depression in rat hippocampal slices and cultures (Nabavi et al., 2013; Aow et al., 2015; Dore et al., 2015, 2016; Gray et al., 2016; Dore et al., 2017; Petit-Pedrol and Groc, 2021). Although the functions of extrasynaptic NMDAR-GluN2B in the primate dlPFC and SGC are completely unknown, our data suggest that events such as those listed above could be more prevalent or frequent in the SGC than the dlPFC.

Implications for vulnerability to depression

The SGC is overactive in patients with depression and is a focus of deep brain stimulation for treating patients with intractable depressive symptoms (Mayberg et al., 2005). The dlPFC provides top regulation of emotion through indirect projections to the SGC (Joyce et al., 2020; Arnsten et al., 2023), and symptoms of depression correlate with synapse loss from the dlPFC (Holmes et al., 2019). Given the extensive outputs of the SGC to the brainstem and subcortical limbic areas, SGC overactivity may have outsized effects on brain states governing emotion and internal states (Hamilton et al., 2015; Arnsten et al., 2023). The dense expression of NMDARs in the SGC (Palomero-Gallagher et al., 2009) has led to the speculation that NMDAR antagonists such as ketamine and esketamine may have antidepressant actions by quieting SGC output, similar to that produced by deep brain stimulation (Opler et al., 2016; Arnsten et al., 2023), especially as ketamine can normalize activity between dlPFC and SGC in marmosets (Alexander et al., 2021). One hypothesis is that NMDAR antagonism is enough to dampen SGC hyperactivity and thus re-balance prefrontal networks and allow top-down regulation to resume (Joermann and Stanton, 2016; Opler et al., 2016; Yang et al., 2021; Arnsten et al., 2023).

It is possible that the extrasynaptic NMDAR-GluN2B in the primate SGC seen in the current study could play a role in depression through their interactions with astrocytes as schematized in Figure 7. The

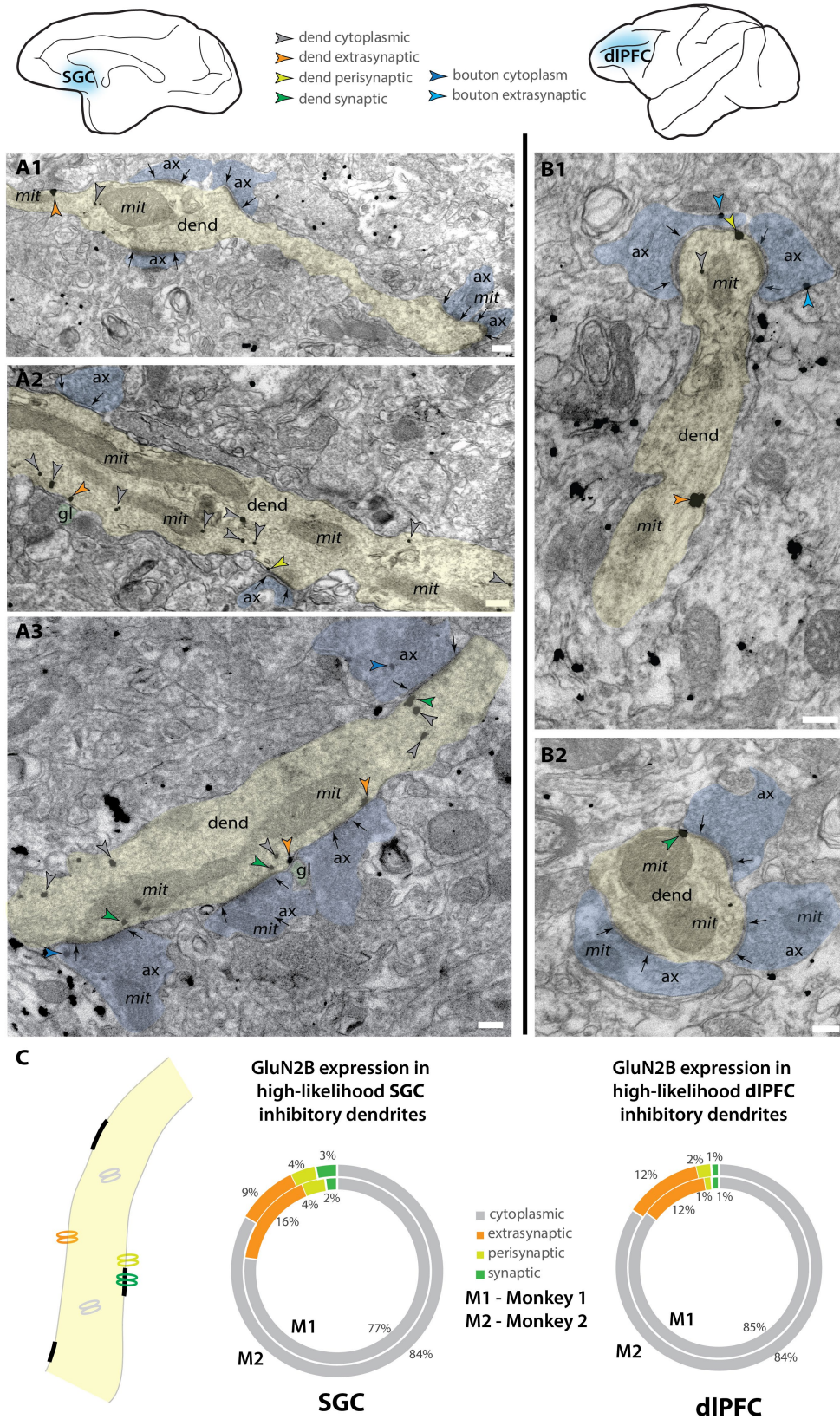
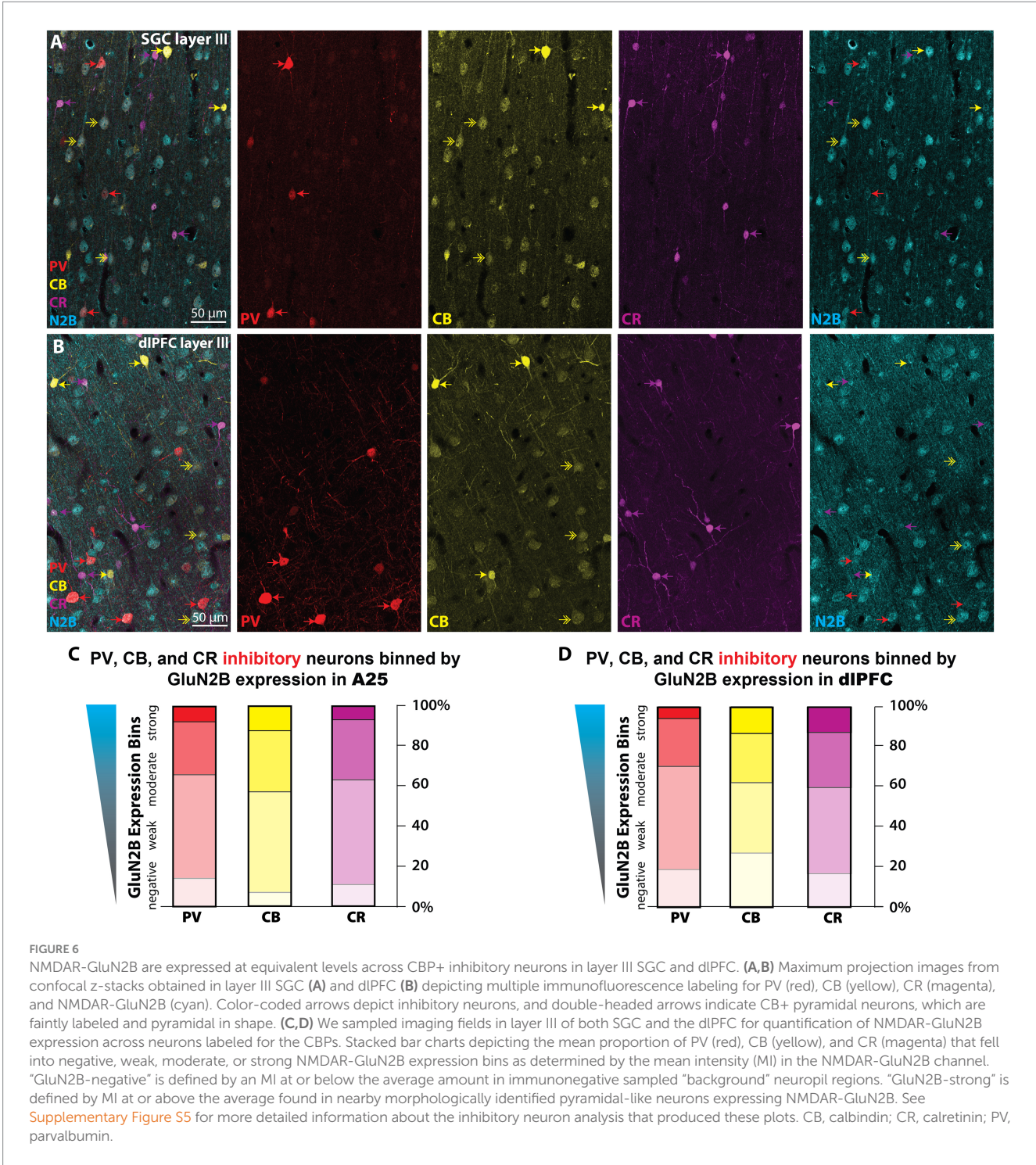


FIGURE 5 NMDAR-GluN2B is expressed in inhibitory dendrites in layer III SGC and dIPFC. Electron micrographs depicting high-likelihood inhibitory dendrites in SGC (A) and dIPFC (B). Dendrites were deemed high-likelihood inhibitory dendrites by the lack of spines in the plane and the presence of two or more asymmetric synapses formed on the dendritic shaft as inhibitory dendrites in the cortex are sparsely spiny or aspiny (Peters et al., 1991). (A1–A3) Examples of NMDAR-GluN2B immunogold labeling in high-likelihood inhibitory dendrites found in layer III SGC. (B1,B2) Examples of NMDAR-GluN2B

(Continued)

FIGURE 5 (Continued)
immunogold labeling in high-likelihood inhibitory dendrites found in layer III dIPFC. **(C)** Nested pie charts depicting the location of NMDAR-GluN2B immunogold particles in high-likelihood dendrites of SGC (left) and dIPFC (right) for Monkey 1 (inside) and Monkey 2 (outside). No statistically significant differences were detected between dIPFC and SGC. Scale bars, 200 nm. ax, axon; dend, dendrite; gl, glial process; mit, mitochondria.



NMDARs have a high affinity for glutamate, allowing them to be engaged at low glutamate concentrations, such as those observed in extracellular space (Sah et al., 1989; Paoletti et al., 2013). Astrocytes

tightly control the concentration of extracellular glutamate via several mechanisms (Cuellar-Santoyo et al., 2022), such as glutamate uptake via the excitatory amino acid transporters (EAATs) (Todd and Hardingham,

2020), glutamate extrusion [e.g., via the cysteine/glutamate antiporter (De Bundel et al., 2011; Lewerenz et al., 2013; Soria et al., 2014)], or even vesicular glutamate release (Bezzi et al., 2004; de Ceglia et al., 2023). In mouse medial PFC (mPFC), extrasynaptic NMDAR-GluN2B are stimulated by a low tonic activation from ambient glutamate, and blocking that tonic NMDAR-GluN2B current abolishes depression-like behaviors while preventing glial uptake of glutamate increases this tonic current (Miller et al., 2014). This suggests that extrasynaptic NMDARs are in equilibrium with glial glutamate transporters and that this balance may govern aspects of mood-like behaviors in mice. Glial pathology has been reported in SGC and other PFC areas in postmortem brains of patients diagnosed with major depression (Ongur et al., 1998; reviewed in Cotter et al., 2001; Rajkowska and Stockmeier, 2013; Haroon et al., 2017; Banasr et al., 2021) as well as in preclinical models (reviewed in Miller et al., 2016). Some studies have found depression-related downregulation of the EAATs (Todd and Hardingham, 2020) in the PFC (Miguel-Hidalgo et al., 2006) and SGC (Scifo et al., 2018), suggesting that they may be less able to regulate extracellular glutamate concentration. Increased extracellular glutamate in depression may engage extrasynaptic NMDAR (Rajkowska and Miguel-Hidalgo, 2007; Miller et al., 2016) to produce despair-like behavior (Miller et al., 2014) and may be a mechanism for SGC hyperactivity (Alexander et al., 2019b; Alexander et al., 2020). Another postmortem study found that the SGC of patients with depression featured an upregulation of quinolinic acid (Steiner et al., 2011), a metabolite of tryptophan produced in glia that acts as an NMDAR agonist (Pedraz-Petrozzi et al., 2020), implying that glial-mediated dysfunction beyond the dysregulation of extracellular glutamate may also occur.

Here, using MLIF and fluorescence intensity analysis, we have detected higher expression of NMDAR-GluN2B in pyramidal neurons than in inhibitory neurons. In both the SGC and dlPFC, we found prominent extrasynaptic NMDAR-GluN2B expression in the dendrites of putative inhibitory neurons of layer III in both SGC and dlPFC, with far lower synaptic expression, especially compared to the nearby spines and dendrites of putative pyramidal dendrites. When present in the synapse, NMDAR-GluN2B were often found only at the very edge of the PSD, suggesting that could fill an ancillary role in second messenger synaptic signaling, rather than contributing prominently to synaptic conductance, in accordance with some findings (Nyiri et al., 2003; Rotaru et al., 2011; reviewed in Miller et al., 2016). Like in pyramidal neurons, in inhibitory neurons, extrasynaptic NMDAR mediates tonic currents in the absence of synaptic stimulation (Povysheva and Johnson, 2012; Riebe et al., 2016). The disinhibition hypothesis of antidepressant action by NMDA antagonists postulates that antagonism of NMDAR on inhibitory neurons provides disinhibition of pyramidal neurons, allowing for renewed plasticity and spine growth in pyramidal neurons (reviewed in Miller et al., 2016; Zanos and Gould, 2018; Brown and Gould, 2024). Our data could suggest that the binding of NMDAR-GluN2B pharmacological agents on dlPFC and SGC layer III inhibitory dendrites may have a predominant effect on extrasynaptic NMDAR rather than synaptic NMDAR, given their higher frequency of expression at extrasynaptic locations. Thus, the disinhibition hypothesis may rely on (i) inhibition of extrasynaptic NMDAR-GluN2B or (ii) inhibition of synaptic NMDAR mediated by other subunits, such as the NMDAR-GluN2C and -GluN2D, which may be more prominent in inhibitory neurons (Paoletti et al., 2013), and ketamine notably has a higher

affinity for these subunits (Kotermanski and Johnson, 2009; Khlestova et al., 2016).

The dlPFC undergoes volume loss and neuronal atrophy in depression, e.g., synapse loss and soma size decrease (Rajkowska et al., 1999; Grieve et al., 2013; Holmes et al., 2019), much like chronic stress-related atrophy found in rodent prelimbic cortex, which has some functional properties in common with dlPFC (Hains et al., 2009). Although the SGC also undergoes general volume loss in depression (Drevets et al., 1997; Botteron et al., 2002), it is unclear how much of that can be attributed to glial atrophy (Ongur et al., 1998). Neurons in rat mPFC that project to the entorhinal cortex exhibit chronic stress-related atrophy, while those that project to the amygdala do not (Shansky et al., 2009), so effects in SGC may be circuit-specific as well. The ultrarapid effects of rapid-acting NMDAR antidepressants may perform an acute role in reducing SGC hyperactivity, perhaps in amygdalar-projecting neurons (Shansky et al., 2009; Joyce et al., 2023), and removing the dominance of SGC in prefrontal networks supporting euthymia and internal states (Hamilton et al., 2015; Opler et al., 2016; Yang et al., 2021; Arnsten et al., 2023). Then, slightly slower effects mediated by antagonism of NMDAR on inhibitory neurons, and subsequent glutamate surge (Abdallah et al., 2018), or by antagonism of synaptic NMDAR activated by spontaneous vesicle release (Zanos and Gould, 2018) may contribute to renewed plasticity in neurons atrophied by chronic stress. These actions are likely critical in re-establishing balance for top-down regions that project to SGC, such as the frontal pole, dlPFC, and pregenual anterior cingulate cortex, that then more slowly reinvigorate spine regrowth and metaplasticity mechanisms across the PFC for sustained remission (Brown and Gould, 2024).

Implications for vulnerability to neurodegenerative forces

Dysregulated calcium signaling has been implicated in the early events leading to sAD (Khachaturian, 1989, 1994; Arnsten et al., 2021c; Datta et al., 2021). Consistent with this hypothesis, the degree of *GRIN2B* expression, and *CALB1* (calbindin) expression in pyramidal cells across the cortical hierarchy roughly aligns with the pattern and sequence of tau pathology in sAD (Braak and Braak, 1991; Garcia-Cabezas et al., 2017; Burt et al., 2018; Yang et al., 2018; Joyce et al., 2020; Arnsten et al., 2021c; Arnsten et al., 2021b; Arnsten and Baudry, 2023). High levels of cytosolic calcium can activate calpain-2 (Wang Y. et al., 2013), which, in turn, activates GSK-3 β and cdk5, the major kinases that hyperphosphorylate tau and exacerbate A β 42 cleavage from APP (reviewed in Arnsten and Baudry, 2023), and amyloid- β toxicity (Kessels et al., 2013; Talantova et al., 2013; Tamburri et al., 2013; Birnbaum et al., 2015). A recent analysis found a loss of synaptic NMDAR-GluN2B and an increase in extrasynaptic NMDAR-GluN2B in the dlPFC of patients with sAD, in line with previous hypotheses that extrasynaptic NMDAR-GluN2B may play a role in sAD etiology (Escamilla et al., 2024). Given that depression is a risk factor for the later development of sAD (Ownby et al., 2006), extrasynaptic NMDAR-GluN2B in the SGC may represent a vulnerable nexus for pathology and mood disorder in both depression and sAD.

Memantine is FDA-approved to treat moderate-to-severe sAD and is a non-competitive antagonist and open channel blocker of the

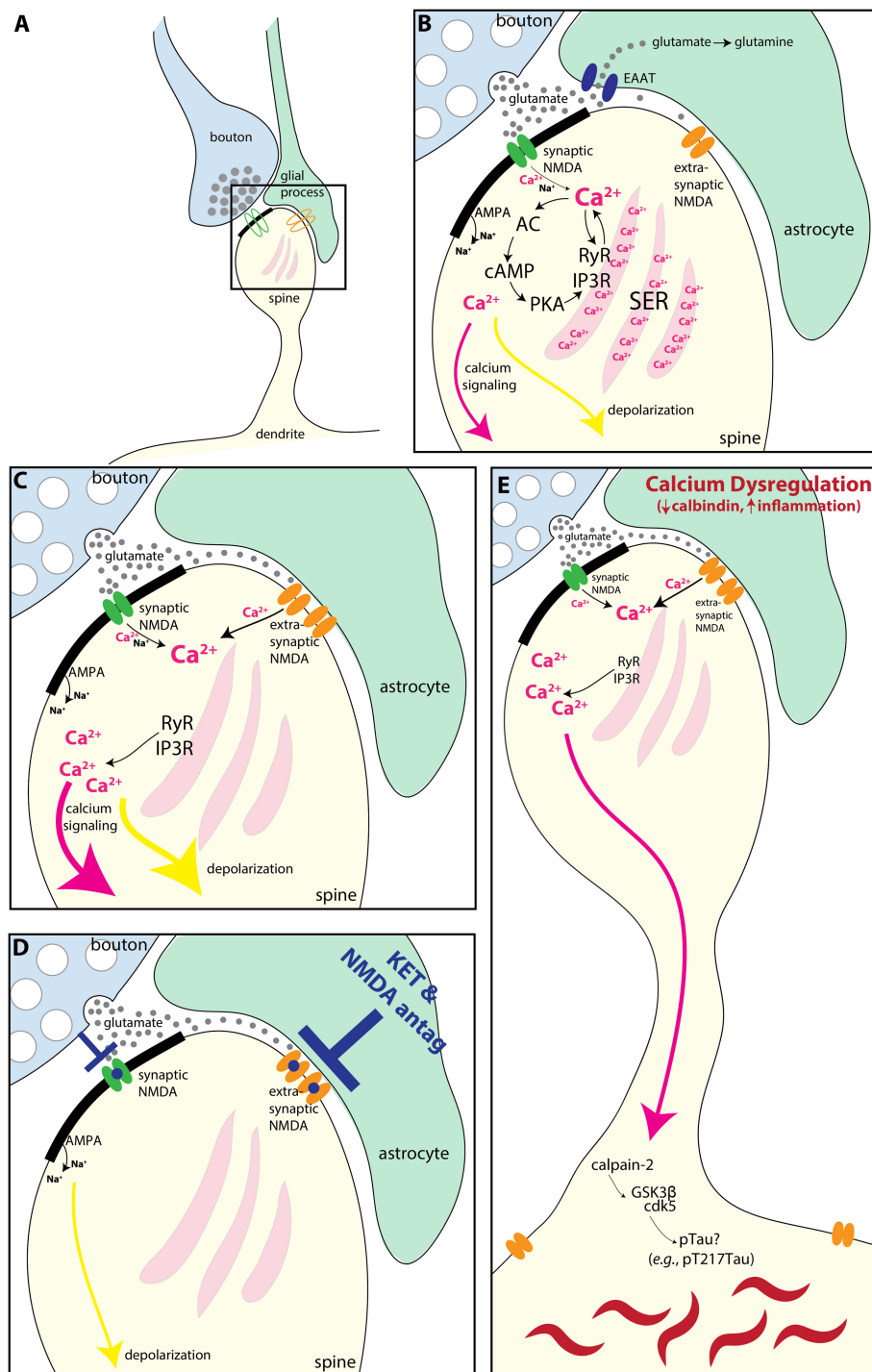


FIGURE 7

Schematic illustrating how extrasynaptic NMDAR-GluN2B may contribute to SGC hyperactivity and/or calcium-mediated neurodegeneration-related events. **(A)** Schematic depicting a spine (yellow), receiving a synapse from a glutamatergic bouton (blue), with an astrocytic leaflet (green) near the synapse. A synaptic NMDAR-GluN2B is present in the synapse (green), and an extrasynaptic NMDAR-GluN2B (orange) is present near the astrocytic process. **(B)** A magnified view showing that the bouton releases glutamate (gray circles) toward the postsynaptic density (thick black band), where the green synaptic NMDAR-GluN2B is engaged and calcium ions (pink), as well as sodium (Na⁺) ions, flow into the spine. AMPA receptors in the postsynaptic density also allow an influx of sodium ions (Na⁺), although these are emphasized less as they are not the focus of the present study. Incoming calcium ions can trigger feedforward calcium release (Berridge, 1998; Arnsten et al., 2021b), via (1) direct calcium-mediated calcium release from the smooth endoplasmic reticulum (SER) by activation of primarily Ryanodine receptors (RyR), and (2) by cAMP magnification of calcium release, whereby calcium activates AC to produce cAMP, which activates PKA signaling. PKA, in turn, phosphorylates the SER calcium channels RyR and IP3R to further increase calcium release. Glutamate escaping out of the synaptic cleft is sequestered into the astrocyte via the EAAT, where it can be converted to glutamine. In the dlPFC, calcium influx can also lead to a reduction in delay-related firing via SK3 channels (Datta et al., 2024) (not shown). **(C)** If the EAATs are perturbed or downregulated, then glutamate can more readily engage extrasynaptic NMDA-GluN2B. Evidence suggests that there may be glial pathology in the SGC during states of depression [(Ongur et al., 1998) reviewed in Cotter et al., 2001, Rajkowska and Stockmeier, 2013, Haroon

(Continued)

FIGURE 7 (Continued)

et al., 2017, and Banasr et al., 2021]. Given the prevalence of extrasynaptic NMDA-GluN2B, we have found in the present study, we hypothesize that these may contribute to SGC hyperactivity observed in depression, perhaps by engaging feedforward calcium mechanisms and increasing depolarization (yellow arrow). (D) Rapid-acting antidepressants that antagonize NMDA receptors may work in part by blocking extrasynaptic NMDAR-GluN2B in the SGC (Miller et al., 2016). (E) Calcium is normally tightly regulated by cytosolic buffering mechanisms (e.g., calbindin and mitochondria) and by phosphodiesterases (which catabolize cAMP). Loss of this regulation with aging and/or inflammation (Arnsten et al., 2021a; Arnsten et al., 2021b; Joyce et al., 2024b) can dysregulate feedforward calcium signaling. Very high levels of cytosolic calcium can activate calpain-2, which cleaves and disinhibits GSK3 β and cdk5, kinases that hyperphosphorylate tau, producing toxic species like pT217Tau (Arnsten and Baudry, 2023). Further post-translational modifications lead to tau fibrillation and the formation of neurofibrillary tangles. AC, adenylyl cyclase; cAMP, cyclic adenosine monophosphate; cdk5, cyclin-dependent kinase 5; EAAT, excitatory amino acid transporter; GSK3 β , glycogen synthase kinase 3 beta; IP3R, inositol triphosphate receptor; PKA, protein kinase A; SER, smooth endoplasmic reticulum spine apparatus; RyR, ryanodine receptor.

NMDARs (Kim et al., 2024). Memantine has at times been thought to target extrasynaptic NMDARs (Xia et al., 2010), although this may be an oversimplification (Glasgow et al., 2017). The lack of benefit from memantine in the early stages of sAD may be due to its antagonism at synaptic NMDAR in dlPFC and related brain circuits that are critical for cognitive processes, thus creating a mixed response profile when combined with inhibition of possibly detrimental extrasynaptic NMDAR signaling. By moderate-to-severe stages of sAD, enough synapse and spine loss may have occurred to attenuate the structural organization of dlPFC microcircuits, thus occluding the detriment due to antagonism of synaptic NMDAR-GluN2B in dlPFC. Memantine has only modest antidepressant effects (Hsu et al., 2022), which may have to do with differential interactions based on subunit composition and desensitization state from nearby high internal calcium concentrations (Glasgow et al., 2017). Understanding the details of NMDAR subtype locations and physiological functions in the primate PFC and cingulate cortices may help to refine treatment strategies for mood and cognitive disorders.

Data availability statement

The raw data supporting the conclusions of this article will be made available by the authors, without undue reservation.

Ethics statement

The animal study was approved by the Yale University Institutional Animal Care & Use Committee. The study was conducted in accordance with the local legislation and institutional requirements.

Author contributions

MKPJ: Writing – original draft, Writing – review & editing, Conceptualization, Formal analysis, Investigation, Methodology. DD: Writing – review & editing, Resources, Methodology. JIA: Writing – review & editing, Resources, Methodology. AD: Writing – review & editing, Resources, Methodology. YMM: Writing – review & editing, Methodology, Resources. JHM: Writing – review & editing, Resources. AFTA: Writing – original draft, Writing – review & editing, Conceptualization, Resources, Supervision.

Funding

The author(s) declare that financial support was received for the research and/or publication of this article. This research was funded by R01 MH130538-01A1 and NSF 2015276 to AFTA.

Acknowledgments

We thank Lisa Ciavarella, Tracy Sadlon, Sam Johnson, and Michelle Wilson for their invaluable contributions.

Conflict of interest

The authors declare that the research was conducted in the absence of any commercial or financial relationships that could be construed as a potential conflict of interest.

The author(s) declared that they were an editorial board member of Frontiers, at the time of submission. This had no impact on the peer review process and the final decision.

Generative AI statement

The authors declare that no Gen AI was used in the creation of this manuscript.

Publisher's note

All claims expressed in this article are solely those of the authors and do not necessarily represent those of their affiliated organizations, or those of the publisher, the editors and the reviewers. Any product that may be evaluated in this article, or claim that may be made by its manufacturer, is not guaranteed or endorsed by the publisher.

Supplementary material

The Supplementary material for this article can be found online at: <https://www.frontiersin.org/articles/10.3389/fnana.2025.1553056/full#supplementary-material>

References

- Abdallah, C. G., De Feyter, H. M., Averill, L. A., Jiang, L., Averill, C. L., Chowdhury, G. M. L., et al. (2018). The effects of ketamine on prefrontal glutamate neurotransmission in healthy and depressed subjects. *Neuropsychopharmacology* 43, 2154–2160. doi: 10.1038/s41386-018-0136-3
- Aggarwal, N. T., and Mielke, M. M. (2023). Sex differences in Alzheimer's disease. *Neurol. Clin.* 41, 343–358. doi: 10.1016/j.ncl.2023.01.001
- Alexander, L., Clarke, H. F., and Roberts, A. C. (2019a). A focus on the functions of area 25. *Brain Sci.* 9:129. doi: 10.3390/brainsci9060129
- Alexander, L., Gaskin, P. L. R., Sawiak, S. J., Fryer, T. D., Hong, Y. T., Cockcroft, G. J., et al. (2019b). Fractionating blunted reward processing characteristic of anhedonia by over-activating primate subgenual anterior cingulate cortex. *Neuron* 101, 307–320. doi: 10.1016/j.neuron.2018.11.021
- Alexander, L., Jelen, L. A., Mehta, M. A., and Young, A. H. (2021). The anterior cingulate cortex as a key locus of ketamine's antidepressant action. *Neurosci. Biobehav. Rev.* 127, 531–554. doi: 10.1016/j.neubiorev.2021.05.003
- Alexander, L., Wood, C. M., Gaskin, P. L. R., Sawiak, S. J., Fryer, T. D., Hong, Y. T., et al. (2020). Over-activation of primate subgenual cingulate cortex enhances the cardiovascular, behavioral and neural responses to threat. *Nat. Commun.* 11:5386. doi: 10.1038/s41467-020-19167-0
- Aow, J., Dore, K., and Malinow, R. (2015). Conformational signaling required for synaptic plasticity by the NMDA receptor complex. *Proc. Natl. Acad. Sci. U. S. A.* 112, 14711–14716. doi: 10.1073/pnas.1520029112
- Arnsten, A. F. T., and Baudry, M. (2023). Targeting Calpain-2 for Alzheimer's disease treatment. *Med. Res. Arch.* 11, 1–12. doi: 10.18103/mra.v11i2.3487
- Arnsten, A. F. T., Datta, D., Del Tredici, K., and Braak, H. (2021c). Hypothesis: tau pathology is an initiating factor in sporadic Alzheimer's disease. *Alzheimers Dement.* 17, 115–124. doi: 10.1002/alz.12192
- Arnsten, A. F. T., Datta, D., and Preuss, T. M. (2021a). Studies of aging nonhuman primates illuminate the etiology of early-stage Alzheimer's-like neuropathology: an evolutionary perspective. *Am. J. Primatol.* 83:e23254. doi: 10.1002/ajp.23254
- Arnsten, A. F. T., Datta, D., and Wang, M. (2021b). The genie in the bottle-magnified calcium signaling in dorsolateral prefrontal cortex. *Mol. Psychiatry* 26, 3684–3700. doi: 10.1038/s41380-020-00973-3
- Arnsten, A. F. T., Joyce, M. K. P., and Roberts, A. C. (2023). The aversive lens: stress effects on the prefrontal-cingulate cortical pathways that regulate emotion. *Neurosci. Biobehav. Rev.* 145:105000. doi: 10.1016/j.neubiorev.2022.105000
- Banasr, M., Sanacora, G., and Esterlis, I. (2021). Macro- and microscale stress-associated alterations in brain structure: translational link with depression. *Biol. Psychiatry* 90, 118–127. doi: 10.1016/j.biopsych.2021.04.004
- Bankhead, P., Loughrey, M. B., Fernández, J. A., Dombrowski, Y., McArt, D. G., Dunne, P. D., et al. (2017). QuPath: open source software for digital pathology image analysis. *Sci. Rep.* 7:16878. doi: 10.1038/s41598-017-17204-5
- Beck, K., Hindley, G., Borgan, F., Ginestet, C., McCutcheon, R., Brugger, S., et al. (2020). Association of Ketamine with psychiatric symptoms and implications for its therapeutic use and for understanding schizophrenia: a systematic review and meta-analysis. *JAMA Netw. Open* 3, e204693. doi: 10.1001/jamanetworkopen.2020.4693
- Berridge, M. J. (1998). Neuronal calcium signaling. *Neuron* 21, 13–26. doi: 10.1016/S0896-6273(00)80510-3
- Bezzi, P., Gunderson, V., Galbete, J. L., Seifert, G., Steinhäuser, C., Pilati, E., et al. (2004). Astrocytes contain a vesicular compartment that is competent for regulated exocytosis of glutamate. *Nat. Neurosci.* 7, 613–620. doi: 10.1038/nn1246
- Birnbaum, J. H., Bali, J., Rajendran, L., Nitsch, R. M., and Tackenberg, C. (2015). Calcium flux-independent NMDA receptor activity is required for A β oligomer-induced synaptic loss. *Cell Death Dis.* 6:e1791. doi: 10.1038/cddis.2015.160
- Botteron, K. N., Raichle, M. E., Drevets, W. C., Heath, A. C., and Todd, R. D. (2002). Volumetric reduction in left subgenual prefrontal cortex in early onset depression. *Biol. Psychiatry* 51, 342–344. doi: 10.1016/s0006-3223(01)01280-x
- Braak, H., and Braak, E. (1991). Neuropathological staging of Alzheimer-related changes. *Acta Neuropathol.* 82, 239–259. doi: 10.1007/BF00308809
- Brown, K. A., and Gould, T. D. (2024). Targeting metaplasticity mechanisms to promote sustained antidepressant actions. *Mol. Psychiatry* 29, 1114–1127. doi: 10.1038/s41380-023-02397-1
- Burt, J. B., Demirtas, M., Eckner, W. J., Navejar, N. M., Ji, J. L., Martin, W. J., et al. (2018). Hierarchy of transcriptomic specialization across human cortex captured by structural neuroimaging topography. *Nat. Neurosci.* 21, 1251–1259. doi: 10.1038/s41593-018-0195-0
- Chalifoux, J. R., and Carter, A. G. (2011). Glutamate spillover promotes the generation of NMDA spikes. *J. Neurosci.* 31, 16435–16446. doi: 10.1523/JNEUROSCI.2777-11.2011
- Chen, A., Sun, Y., Lei, Y., Li, C., Liao, S., Meng, J., et al. (2023). Single-cell spatial transcriptome reveals cell-type organization in the macaque cortex. *Cell* 186, 3726–3743. doi: 10.1016/j.cell.2023.06.009
- Conde, F., Lund, J. S., Jacobowitz, D. M., Baimbridge, K. G., and Lewis, D. A. (1994). Local circuit neurons immunoreactive for calretinin, calbindin D-28k or parvalbumin in monkey prefrontal cortex: distribution and morphology. *J. Comp. Neurol.* 341, 95–116. doi: 10.1002/cne.903410109
- Cotter, D. R., Pariante, C. M., and Everall, I. P. (2001). Glial cell abnormalities in major psychiatric disorders: the evidence and implications. *Brain Res. Bull.* 55, 585–595. doi: 10.1016/S0361-9230(01)00527-5
- Cuellar-Santoyo, A. O., Ruiz-Rodríguez, V. M., Mares-Barbosa, T. B., Patrón-Soberano, A., Howe, A. G., Portales-Pérez, D. P., et al. (2022). Revealing the contribution of astrocytes to glutamatergic neuronal transmission. *Front. Cell. Neurosci.* 16:1037641. doi: 10.3389/fncel.2022.1037641
- Datta, D., Leslie, S. N., Wang, M., Morozov, Y. M., Yang, S., Mentone, S., et al. (2021). Age-related calcium dysregulation linked with tau pathology and impaired cognition in non-human primates. *Alzheimers Dement.* 17, 920–932. doi: 10.1002/alz.12325
- Datta, D., Yang, S., Joyce, M. K. P., Woo, E., McCarroll, S. A., Gonzalez-Burgos, G., et al. (2024). Key roles of CACNA1C/Cav 1.2 and CALB1/Calbindin in prefrontal neurons altered in cognitive disorders. *JAMA Psychiatry* 81:870. doi: 10.1001/jamapsychiatry.2024.1112
- De Bundel, D., Schallier, A., Loyens, E., Fernando, R., Miyashita, H., Van Liefvering, J., et al. (2011). Loss of system x (c)- does not induce oxidative stress but decreases extracellular glutamate in hippocampus and influences spatial working memory and limbic seizure susceptibility. *J. Neurosci.* 31, 5792–5803. doi: 10.1523/JNEUROSCI.5465-10.2011
- de Ceglia, R., Ledonne, A., Litvin, D. G., Lind, B. L., Carriero, G., Latagliata, E. C., et al. (2023). Specialized astrocytes mediate glutamatergic gliotransmission in the CNS. *Nature* 622, 120–129. doi: 10.1038/s41586-023-06502-w
- DeFelipe, J. (1997). Types of neurons, synaptic connections and chemical characteristics of cells immunoreactive for calbindin-D28K, parvalbumin and calretinin in the neocortex. *J. Chem. Neuroanat.* 14, 1–19. doi: 10.1016/S0891-0618(97)10013-8
- Dore, K., Aow, J., and Malinow, R. (2015). Agonist binding to the NMDA receptor drives movement of its cytoplasmic domain without ion flow. *Proc. Natl. Acad. Sci. U. S. A.* 112, 14705–14710. doi: 10.1073/pnas.1520023112
- Dore, K., Aow, J., and Malinow, R. (2016). The emergence of NMDA receptor metabotropic function: insights from imaging. *Front. Synaptic Neurosci.* 8:20. doi: 10.3389/fnsyn.2016.00020
- Dore, K., Stein, I. S., Brock, J. A., Castillo, P. E., Zito, K., and Sjöström, P. J. (2017). Unconventional NMDA receptor signaling. *J. Neurosci.* 37, 10800–10807. doi: 10.1523/JNEUROSCI.1825-17.2017
- Drevets, W. C., Price, J. L., Simpson, J. R. Jr., Todd, R. D., Reich, T., Vannier, M., et al. (1997). Subgenual prefrontal cortex abnormalities in mood disorders. *Nature* 386, 824–827. doi: 10.1038/386824a0
- Erreger, K., Dravid, S. M., Banke, T. G., Wyllie, D. J., and Traynelis, S. F. (2005). Subunit-specific gating controls rat NR1/NR2A and NR1/NR2B NMDA channel kinetics and synaptic signalling profiles. *J. Physiol.* 563, 345–358. doi: 10.1113/jphysiol.2004.080028
- Escamilla, S., Badillos, R., Comella, J. X., Solé, M., Pérez-Otaño, I., Mut, J. V. S., et al. (2024). Synaptic and extrasynaptic distribution of NMDA receptors in the cortex of Alzheimer's disease patients. *Alzheimers Dement.* 20, 8231–8245. doi: 10.1002/alz.14125
- Fellin, T., Pascual, O., Gobbo, S., Pozzan, T., Haydon, P. G., and Carmignoto, G. (2004). Neuronal synchrony mediated by astrocytic glutamate through activation of extrasynaptic NMDA receptors. *Neuron* 43, 729–743. doi: 10.1016/j.neuron.2004.08.011
- Fiala, J. C. (2005). Reconstruct: a free editor for serial section microscopy. *J. Microsc.* 218, 52–61. doi: 10.1111/j.1365-2818.2005.01466.x
- García-Cabezas, M. A., Joyce, M. P., John, Y., Zikopoulos, B., and Barbas, H. (2017). Mirror trends of plasticity and stability indicators in primate prefrontal cortex. *Eur. J. Neurosci.* 46, 2392–2405. doi: 10.1111/ejn.13706
- Gladding, C. M., and Raymond, L. A. (2011). Mechanisms underlying NMDA receptor synaptic/extrasynaptic distribution and function. *Mol. Cell. Neurosci.* 48, 308–320. doi: 10.1016/j.mcn.2011.05.001
- Glasgow, N. G., Povysheva, N. V., Azofeifa, A. M., and Johnson, J. W. (2017). Memantine and ketamine differentially alter NMDA receptor desensitization. *J. Neurosci.* 37, 9686–9704. doi: 10.1523/JNEUROSCI.1173-17.2017
- Glasgow, N. G., Siegler Retchless, B., and Johnson, J. W. (2015). Molecular bases of NMDA receptor subtype-dependent properties. *J. Physiol.* 593, 83–95. doi: 10.1113/jphysiol.2014.273763
- Gray, J. A., Zito, K., and Hell, J. W. (2016). Non-ionic signaling by the NMDA receptor: controversy and opportunity. *F1000Res* 5:1010. doi: 10.12688/f1000research.8366.1
- Grieve, S. M., Korgaonkar, M. S., Koslow, S. H., Gordon, E., and Williams, L. M. (2013). Widespread reductions in gray matter volume in depression. *Neuro Image Clin.* 3, 332–339. doi: 10.1016/j.nicl.2013.08.016
- Groc, L., and Choquet, D. (2020). Linking glutamate receptor movements and synapse function. *Science* 368:eaay4631. doi: 10.1126/science.aay4631
- Hains, A. B., Vu, M. A., Maciejewski, P. K., van Dyck, C. H., Gottron, M., and Arnsten, A. F. (2009). Inhibition of protein kinase C signaling protects prefrontal cortex

- dendritic spines and cognition from the effects of chronic stress. *Proc. Natl. Acad. Sci. U. S. A.* 106, 17957–17962. doi: 10.1073/pnas.0908563106
- Hamilton, J. P., Farmer, M., Fogelman, P., and Gotlib, I. H. (2015). Depressive rumination, the default-mode network, and the dark matter of clinical neuroscience. *Biol. Psychiatry* 78, 224–230. doi: 10.1016/j.biopsych.2015.02.020
- Hardingham, G. E., and Bading, H. (2010). Synaptic versus extrasynaptic NMDA receptor signalling: implications for neurodegenerative disorders. *Nat. Rev. Neurosci.* 11, 682–696. doi: 10.1038/nrn2911
- Hardingham, G. E., Fukunaga, Y., and Bading, H. (2002). Extrasynaptic NMDARs oppose synaptic NMDARs by triggering CREB shut-off and cell death pathways. *Nat. Neurosci.* 5, 405–414. doi: 10.1038/nrn835
- Haroon, E., Miller, A. H., and Sanacora, G. (2017). Inflammation, glutamate, and glia: a trio of trouble in mood disorders. *Neuropsychopharmacology* 42, 193–215. doi: 10.1038/npp.2016.199
- Harris, A. Z., and Pettit, D. L. (2007). Extrasynaptic and synaptic NMDA receptors form stable and uniform pools in rat hippocampal slices. *J. Physiol.* 584, 509–519. doi: 10.1113/jphysiol.2007.137679
- Hof, P. R., and Morrison, J. H. (1991). Neocortical neuronal subpopulations labeled by a monoclonal antibody to calbindin exhibit differential vulnerability in Alzheimer's disease. *Exp. Neurol.* 111, 293–301. doi: 10.1016/0014-4886(91)90096-U
- Holmes, S. E., Scheinost, D., Finnema, S. J., Naganawa, M., Davis, M. T., Della Gioia, N., et al. (2019). Lower synaptic density is associated with depression severity and network alterations. *Nat. Commun.* 10, 1529. doi: 10.1038/s41467-019-09562-7
- Hsu, T. W., Chu, C. S., Ching, P. Y., Chen, G. W., and Pan, C. C. (2022). The efficacy and tolerability of memantine for depressive symptoms in major mental diseases: a systematic review and updated meta-analysis of double-blind randomized controlled trials. *J. Affect. Disord.* 306, 182–189. doi: 10.1016/j.jad.2022.03.047
- Hsu, A., Luebke, J. I., and Medalla, M. (2017). Comparative ultrastructural features of excitatory synapses in the visual and frontal cortices of the adult mouse and monkey. *J. Comp. Neurol.* 525, 2175–2191. doi: 10.1002/cne.24196
- Jormann, J., and Stanton, C. H. (2016). Examining emotion regulation in depression: a review and future directions. *Behav. Res. Ther.* 86, 35–49. doi: 10.1016/j.brat.2016.07.007
- Joyce, M. K. P., Garcia-Cabezas, M. A., John, Y. J., and Barbas, H. (2020). Serial prefrontal pathways are positioned to balance cognition and emotion in Primates. *J. Neurosci.* 40, 8306–8328. doi: 10.1523/JNEUROSCI.0860-20.2020
- Joyce, M. K. P., Ivanov, T., Krienen, F., Mitchell, J., Ma, S., Inoue, W., et al. (2024a). Dopamine D1 receptor expression in dlPFC inhibitory parvalbumin neurons may contribute to higher visuospatial distractibility in marmosets versus macaques. *bioRxiv [Preprint]*. 97, 359–371. doi: 10.1101/2024.06.15.599163
- Joyce, M. K. P., Uchendu, S., and Arnsten, A. F. T. (2024b). Stress and inflammation target dorsolateral prefrontal cortex function: neural mechanisms underlying weakened cognitive control. *Biol. Psychiatry*. 97, 359–371. doi: 10.1016/j.biopsych.2024.06.016
- Joyce, M. K. P., Wang, J., and Barbas, H. (2023). Subgenual and hippocampal pathways in amygdala are set to balance affect and context processing. *J. Neurosci.* 43, 3061–3080. doi: 10.1523/JNEUROSCI.2066-22.2023
- Kessels, H. W., Nabavi, S., and Malinow, R. (2013). Metabotropic NMDA receptor function is required for β -amyloid-induced synaptic depression. *Proc. Natl. Acad. Sci. USA* 110, 4033–4038. doi: 10.1073/pnas.1219605110
- Khachaturian, Z. S. (1989). Calcium, membranes, aging, and Alzheimer's disease. Introduction and overview. *Ann. N. Y. Acad. Sci.* 568, 1–4. doi: 10.1111/j.1749-6632.1989.tb12485.x
- Khachaturian, Z. S. (1994). Calcium hypothesis of Alzheimer's disease and brain aging. *Ann. N. Y. Acad. Sci.* 747, 1–11. doi: 10.1111/j.1749-6632.1994.tb44398.x
- Khlestova, E., Johnson, J. W., Krystal, J. H., and Lisman, J. (2016). The role of Glu N2C-containing NMDA receptors in Ketamine's psychotogenic action and in schizophrenia models. *J. Neurosci.* 36, 11151–11157. doi: 10.1523/JNEUROSCI.1203-16.2016
- Kim, A. Y., Al Jerdi, S., Mac Donald, R., and Triggie, C. R. (2024). Alzheimer's disease and its treatment-yesterday, today, and tomorrow. *Front. Pharmacol.* 15, 1399121. doi: 10.3389/fphar.2024.1399121
- Kondo, H., Tanaka, K., Hashikawa, T., and Jones, E. G. (1999). Neurochemical gradients along monkey sensory cortical pathways: calbindin-immunoreactive pyramidal neurons in layers II and III. *Eur. J. Neurosci.* 11, 4197–4203. doi: 10.1046/j.1460-9568.1999.00844.x
- Kortus, S., Rehakova, K., Klima, M., Kolcheva, M., Ladislav, M., Langore, E., et al. (2023). Subunit-dependent surface mobility and localization of NMDA receptors in hippocampal neurons measured using Nanobody probes. *J. Neurosci.* 43, 4755–4774. doi: 10.1523/JNEUROSCI.2014-22.2023
- Kotermanski, S. E., and Johnson, J. W. (2009). Mg²⁺ imparts NMDA receptor subtype selectivity to the Alzheimer's drug memantine. *J. Neurosci.* 29, 2774–2779. doi: 10.1523/JNEUROSCI.3703-08.2009
- Krystal, J. H., Kavalali, E. T., and Monteggia, L. M. (2024). Ketamine and rapid antidepressant action: new treatments and novel synaptic signaling mechanisms. *Neuropsychopharmacology* 49, 41–50. doi: 10.1038/s41386-023-01629-w
- Lewerenz, J., Hewett, S. J., Huang, Y., Lambros, M., Gout, P. W., Kalivas, P. W., et al. (2013). The cystine/glutamate antiporter system x (c) (–) in health and disease: from molecular mechanisms to novel therapeutic opportunities. *Antioxid. Redox Signal.* 18, 522–555. doi: 10.1089/ars.2011.4391
- Lisman, J. E., Fellous, J. M., and Wang, X. J. (1998). A role for NMDA-receptor channels in working memory. *Nat. Neurosci.* 1, 273–275. doi: 10.1038/1086
- Mayberg, H. S., Lozano, A. M., Voon, V., McNeely, H. E., Seminowicz, D., Hamani, C., et al. (2005). Deep brain stimulation for treatment-resistant depression. *Neuron* 45, 651–660. doi: 10.1016/j.neuron.2005.02.014
- Medalla, M., Mo, B., Nasar, R., Zhou, Y., Park, J., and Luebke, J. I. (2023). Comparative features of calretinin, calbindin, and parvalbumin expressing interneurons in mouse and monkey primary visual and frontal cortices. *J. Comp. Neurol.* 531, 1934–1962. doi: 10.1002/cne.25514
- Miguel-Hidalgo, J. J., Overholser, J. C., Meltzer, H. Y., Stockmeier, C. A., and Rajkowska, G. (2006). Reduced glial and neuronal packing density in the orbitofrontal cortex in alcohol dependence and its relationship with suicide and duration of alcohol dependence. *Alcohol. Clin. Exp. Res.* 30, 1845–1855. doi: 10.1111/j.1530-0277.2006.00221.x
- Miller, O. H., Moran, J. T., and Hall, B. J. (2016). Two cellular hypotheses explaining the initiation of ketamine's antidepressant actions: direct inhibition and disinhibition. *Neuropharmacology* 100, 17–26. doi: 10.1016/j.neuropharm.2015.07.028
- Miller, O. H., Yang, L., Wang, C. C., Hargroder, E. A., Zhang, Y., Delpire, E., et al. (2014). Glu N2B-containing NMDA receptors regulate depression-like behavior and are critical for the rapid antidepressant actions of ketamine. *Elife* 3:e03581. doi: 10.7554/eLife.03581
- Muntané, G., Horvath, J. E., Hof, P. R., Ely, J. J., Hopkins, W. D., Raghanti, M. A., et al. (2015). Analysis of synaptic gene expression in the neocortex of primates reveals evolutionary changes in glutamatergic neurotransmission. *Cereb. Cortex* 25, 1596–1607. doi: 10.1093/cercor/bht354
- Murray, J. D., Bernacchia, A., Freedman, D. J., Romo, R., Wallis, J. D., Cai, X., et al. (2014). A hierarchy of intrinsic timescales across primate cortex. *Nat. Neurosci.* 17, 1661–1663. doi: 10.1038/nn.3862
- Nabavi, S., Kessels, H. W., Alfonso, S., Aow, J., Fox, R., and Malinow, R. (2013). Metabotropic NMDA receptor function is required for NMDA receptor-dependent long-term depression. *Proc. Natl. Acad. Sci. U. S. A.* 110, 4027–4032. doi: 10.1073/pnas.1219454110
- Newpher, T. M., and Ehlers, M. D. (2008). Glutamate receptor dynamics in dendritic microdomains. *Neuron* 58, 472–497. doi: 10.1016/j.neuron.2008.04.030
- Nyiri, G., Stephenson, F. A., Freund, T. F., and Somogyi, P. (2003). Large variability in synaptic N-methyl-D-aspartate receptor density on interneurons and a comparison with pyramidal-cell spines in the rat hippocampus. *Neuroscience* 119, 347–363. doi: 10.1016/S0306-4522(03)00157-X
- Ongur, D., Drevets, W. C., and Price, J. L. (1998). Glial reduction in the subgenual prefrontal cortex in mood disorders. *Proc. Natl. Acad. Sci. U. S. A.* 95, 13290–13295. doi: 10.1073/pnas.95.22.13290
- Opler, L. A., Opler, M. G., and Arnsten, A. F. (2016). Ameliorating treatment-refractory depression with intranasal ketamine: potential NMDA receptor actions in the pain circuitry representing mental anguish. *CNS Spectr.* 21, 12–22. doi: 10.1017/S1092852914000686
- Ownby, R. L., Crocco, E., Acevedo, A., John, V., and Loewenstein, D. (2006). Depression and risk for Alzheimer disease: systematic review, meta-analysis, and metaregression analysis. *Arch. Gen. Psychiatry* 63, 530–538. doi: 10.1001/archpsyc.63.5.530
- Palmer, L. M., Shai, A. S., Reeve, J. E., Anderson, H. L., Paulsen, O., and Larkum, M. E. (2014). NMDA spikes enhance action potential generation during sensory input. *Nat. Neurosci.* 17, 383–390. doi: 10.1038/nn.3646
- Palomero-Gallagher, N., Vogt, B. A., Schleicher, A., Mayberg, H. S., and Zilles, K. (2009). Receptor architecture of human cingulate cortex: evaluation of the four-region neurobiological model. *Hum. Brain Mapp.* 30, 2336–2355. doi: 10.1002/hbm.20667
- Paoletti, P., Bellone, C., and Zhou, Q. (2013). NMDA receptor subunit diversity: impact on receptor properties, synaptic plasticity and disease. *Nat. Rev. Neurosci.* 14, 383–400. doi: 10.1038/nrn3504
- Papouin, T., Ladepeche, L., Ruel, J., Sacchi, S., Labasque, M., Hanini, M., et al. (2012). Synaptic and extrasynaptic NMDA receptors are gated by different endogenous coagonists. *Cell* 150, 633–646. doi: 10.1016/j.cell.2012.06.029
- Parri, H. R., Gould, T. M., and Crunelli, V. (2001). Spontaneous astrocytic Ca²⁺ oscillations in situ drive NMDAR-mediated neuronal excitation. *Nat. Neurosci.* 4, 803–812. doi: 10.1038/90507
- Parsons, M. P., and Raymond, L. A. (2014). Extrasynaptic NMDA receptor involvement in central nervous system disorders. *Neuron* 82, 279–293. doi: 10.1016/j.neuron.2014.03.030
- Pedraz-Petrozzi, B., Elyamany, O., Rummel, C., and Mulert, C. (2020). Effects of inflammation on the kynurenine pathway in schizophrenia - a systematic review. *J. Neuroinflammation* 17:56. doi: 10.1186/s12974-020-1721-z
- Peters, A., Palay, S. L., and Webster, H. D. (1991). The fine structure of the nervous system. Neurons and their supporting cells. 3rd Edn. New York: Oxford University Press.
- Petit-Pedrol, M., and Groc, L. (2021). Regulation of membrane NMDA receptors by dynamics and protein interactions. *J. Cell Biol.* 220:e202006101. doi: 10.1083/jcb.202006101
- Petralia, R. S. (2012). Distribution of extrasynaptic NMDA receptors on neurons. *Sci. World J.* 2012:267120, 1–11. doi: 10.1100/2012/267120

- Petralia, R. S., and Wang, Y. X. (2021). Review of post-embedding immunogold methods for the study of neuronal structures. *Front. Neuroanat.* 15:763427. doi: 10.3389/fnana.2021.763427
- Petralia, R. S., Wang, Y. X., Hua, F., Yi, Z., Zhou, A., Ge, L., et al. (2010). Organization of NMDA receptors at extrasynaptic locations. *Neuroscience* 167, 68–87. doi: 10.1016/j.neuroscience.2010.01.022
- Poskanzer, K. E., and Yuste, R. (2016). Astrocytes regulate cortical state switching in vivo. *Proc. Natl. Acad. Sci. U. S. A.* 113, E2675–E2684. doi: 10.1073/pnas.1520759113
- Povyshva, N. V., and Johnson, J. W. (2012). Tonic NMDA receptor-mediated current in prefrontal cortical pyramidal cells and fast-spiking interneurons. *J. Neurophysiol.* 107, 2232–2243. doi: 10.1152/jn.01017.2011
- Rajkowska, G., and Miguel-Hidalgo, J. J. (2007). Gliogenesis and glial pathology in depression. *CNS Neurol. Disord. Drug Targets* 6, 219–233. doi: 10.2174/187152707780619326
- Rajkowska, G., Miguel-Hidalgo, J. J., Wei, J., Dilley, G., Pittman, S. D., Meltzer, H. Y., et al. (1999). Morphometric evidence for neuronal and glial prefrontal cell pathology in major depression. *Biol. Psychiatry* 45, 1085–1098. doi: 10.1016/S0006-3223(99)00041-4
- Rajkowska, G., and Stockmeier, C. A. (2013). Astrocyte pathology in major depressive disorder: insights from human postmortem brain tissue. *Curr. Drug Targets* 14, 1225–1236. doi: 10.2174/13894501113149990156
- Rhodes, P. (2006). The properties and implications of NMDA spikes in neocortical pyramidal cells. *J. Neurosci.* 26, 6704–6715. doi: 10.1523/JNEUROSCI.3791-05.2006
- Riebe, L., Seth, H., Culley, G., Dósa, Z., Radi, S., Strand, K., et al. (2016). Tonic active NMDA receptors – a signalling mechanism critical for interneuronal excitability in the CA1 stratum radiatum. *Eur. J. Neurosci.* 43, 169–178. doi: 10.1111/ejn.13128
- Rotaru, D. C., Yoshino, H., Lewis, D. A., Ermentrout, G. B., and Gonzalez-Burgos, G. (2011). Glutamate receptor subtypes mediating synaptic activation of prefrontal cortex neurons: relevance for schizophrenia. *J. Neurosci.* 31, 142–156. doi: 10.1523/JNEUROSCI.1970-10.2011
- Sah, P., Hestrin, S., and Nicoll, R. A. (1989). Tonic activation of NMDA receptors by ambient glutamate enhances excitability of neurons. *Science* 246, 815–818. doi: 10.1126/science.2573153
- Schwitzer, B., Singh, J., Fejtova, A., Groc, L., Heine, M., and Frischknecht, R. (2017). Hyaluronic acid based extracellular matrix regulates surface expression of Glu N2B containing NMDA receptors. *Sci. Rep.* 7:10991. doi: 10.1038/s41598-017-07003-3
- Scifo, E., Pabba, M., Kapadia, F., Ma, T., Lewis, D. A., Tseng, G. C., et al. (2018). Sustained molecular pathology across episodes and remission in major depressive disorder. *Biol. Psychiatry* 83, 81–89. doi: 10.1016/j.biopsych.2017.08.008
- Seney, M. L., Huo, Z., Cahill, K., French, L., Puralewski, R., Zhang, J., et al. (2018). Opposite molecular signatures of depression in men and women. *Biol. Psychiatry* 84, 18–27. doi: 10.1016/j.biopsych.2018.01.017
- Seney, M. L., and Sibille, E. (2014). Sex differences in mood disorders: perspectives from humans and rodent models. *Biol. Sex Differ.* 5:17. doi: 10.1186/s13293-014-0017-3
- Shansky, R. M., Hamo, C., Hof, P. R., McEwen, B. S., and Morrison, J. H. (2009). Stress-induced dendritic remodeling in the prefrontal cortex is circuit specific. *Cereb. Cortex* 19, 2479–2484. doi: 10.1093/cercor/bhp003
- Shansky, R. M., Rubinow, K., Brennan, A., and Arnsten, A. F. (2006). The effects of sex and hormonal status on restraint-stress-induced working memory impairment. *Behav. Brain Funct.* 2:8. doi: 10.1186/1744-9081-2-8
- Soria, F. N., Pérez-Samartín, A., Martín, A., Gona, K. B., Llop, J., Szczupak, B., et al. (2014). Extrasynaptic glutamate release through cystine/glutamate antiporter contributes to ischemic damage. *J. Clin. Invest.* 124, 3645–3655. doi: 10.1172/JCI71886
- Steiner, J., Walter, M., Gos, T., Guillemin, G. J., Bernstein, H. G., Sarnyai, Z., et al. (2011). Severe depression is associated with increased microglial quinolinic acid in subregions of the anterior cingulate gyrus: evidence for an immune-modulated glutamatergic neurotransmission? *J. Neuroinflammation* 8:94. doi: 10.1186/1742-2094-8-94
- Talantova, M., Sanz-Blasco, S., Zhanga, X., Xia, P., Akhtara, M. W., Okamoto, S., et al. (2013). Abeta induces astrocytic glutamate release, extrasynaptic NMDA receptor activation, and synaptic loss. *Proc. Natl. Acad. Sci. U. S. A.* 110, E2518–E2527. doi: 10.1073/pnas.1306832110
- Tamburri, A., Dudilot, A., Licea, S., Bourgeois, C., and Boehm, J. (2013). NMDA-receptor activation but not ion flux is required for amyloid-beta induced synaptic depression. *PLoS One* 8:e65350. doi: 10.1371/journal.pone.0065350
- Telezhkin, V., Schnell, C., Yarova, P., Yung, S., Cope, E., Hughes, A., et al. (2016). Forced cell cycle exit and modulation of GABAA, CREB, and GSK3 β signaling promote functional maturation of induced pluripotent stem cell-derived neurons. *Am. J. Phys. Cell Phys.* 310, C520–C541. doi: 10.1152/ajpcell.00166.2015
- Testa-Silva, G., Rosier, M., Honnuraiah, S., Guzulaitis, R., Megias, A. M., French, C., et al. (2022). High synaptic threshold for dendritic NMDA spike generation in human layer 2/3 pyramidal neurons. *Cell Rep.* 41:111787. doi: 10.1016/j.celrep.2022.111787
- Thomas, C. G., Miller, A. J., and Westbrook, G. L. (2006). Synaptic and extrasynaptic NMDA receptor NR2 subunits in cultured hippocampal neurons. *J. Neurophysiol.* 95, 1727–1734. doi: 10.1152/jn.00771.2005
- Todd, A. C., and Hardingham, G. E. (2020). The regulation of astrocytic glutamate transporters in health and neurodegenerative diseases. *Int. J. Mol. Sci.* 21:9607. doi: 10.3390/ijms21249607
- Tovar, K. R., and Westbrook, G. L. (1999). The incorporation of NMDA receptors with a distinct subunit composition at nascent hippocampal synapses in vitro. *J. Neurosci.* 19, 4180–4188. doi: 10.1523/JNEUROSCI.19-10-04180.1999
- Tsolias, A., and Medalla, M. (2021). Muscarinic acetylcholine receptor localization on distinct excitatory and inhibitory neurons within the ACC and LPFC of the Rhesus monkey. *Front. Neural Circ.* 15:795325. doi: 10.3389/fncir.2021.795325
- Wang, Y., Briz, V., Chishti, A., Bi, X., and Baudry, M. (2013). Distinct roles for m-calpain and m-calpain in synaptic NMDAR-mediated neuroprotection and extrasynaptic NMDAR-mediated neurodegeneration. *J. Neurosci.* 33, 18880–18892. doi: 10.1523/JNEUROSCI.3293-13.2013
- Wang, M., Yang, Y., Wang, C. J., Gamo, N. J., Jin, L. E., Mazer, J. A., et al. (2013). NMDA receptors subserve persistent neuronal firing during working memory in dorsolateral prefrontal cortex. *Neuron* 77, 736–749. doi: 10.1016/j.neuron.2012.12.032
- Wyllie, D. J., Livesey, M. R., and Hardingham, G. E. (2013). Influence of Glu N2 subunit identity on NMDA receptor function. *Neuropharmacology* 74, 4–17. doi: 10.1016/j.neuropharm.2013.01.016
- Xia, P., Chen, H. S., Zhang, D., and Lipton, S. A. (2010). Memantine preferentially blocks extrasynaptic over synaptic NMDA receptor currents in hippocampal autapses. *J. Neurosci.* 30, 11246–11250. doi: 10.1523/JNEUROSCI.2488-10.2010
- Yang, S., Seo, H., Wang, M., and Arnsten, A. F. T. (2021). NMDAR neurotransmission needed for persistent neuronal firing: potential roles in mental disorders. *Front. Psychiat.* 12:654322. doi: 10.3389/fpsy.2021.654322
- Yang, S. T., Wang, M., Paspalas, C. D., Crimins, J. L., Altman, M. T., Mazer, J. A., et al. (2018). Core differences in synaptic signaling between primary visual and dorsolateral prefrontal cortex. *Cereb. Cortex* 28, 1458–1471. doi: 10.1093/cercor/bhx357
- Zanos, P., and Gould, T. D. (2018). Mechanisms of ketamine action as an antidepressant. *Mol. Psychiatry* 23, 801–811. doi: 10.1038/mp.2017.255
- Zong, P., Feng, J., Yue, Z., Li, Y., Wu, G., Sun, B., et al. (2022). Functional coupling of TRPM2 and extrasynaptic NMDARs exacerbates excitotoxicity in ischemic brain injury. *Neuron* 110, 1944–1958.e48.